

1 Multiple sources of slow activity fluctuations in a bacterial

2 chemosensory network

3 R. Colin^{1,*,+}, C. Rosazza^{1,*}, A. Vaknin², V. Sourjik^{1,+}

4 ¹Max Planck Institute for Terrestrial Microbiology and LOEWE Center for Synthetic
5 Microbiology (SYNMIKRO), Karl-von-Frisch-Strasse 16, D-35043 Marburg, Germany

6 ²The Racah Institute of Physics, the Hebrew University, Jerusalem 91904, Israel

7 * Authors contributed equally to this work.

8 ⁺ Corresponding authors: victor.sourjik@synmikro.mpi-marburg.mpg.de,

9 remy.colin@synmikro.mpi-marburg.mpg.de

10

11 Abstract

12 Cellular networks are intrinsically subject to stochastic fluctuations, but analysis of the resulting
13 noise remained largely limited to gene expression. The pathway controlling chemotaxis of
14 *Escherichia coli* provides one example where posttranslational signaling noise has been deduced
15 from cellular behavior. This noise was proposed to result from stochasticity in chemoreceptor
16 methylation, and it is believed to enhance environment exploration by bacteria. Here we
17 combined single-cell FRET measurements with analysis based on the fluctuation-dissipation
18 theorem (FDT) to characterize origins of activity fluctuations within the chemotaxis pathway.
19 We observed surprisingly large methylation-independent thermal fluctuations of receptor
20 activity, which contribute to noise comparably to the energy-consuming methylation dynamics.
21 Interactions between clustered receptors involved in amplification of chemotactic signals are also
22 necessary to produce the observed large activity fluctuations. Our work thus shows that the high

23 response sensitivity of this cellular pathway also increases its susceptibility to noise, from
24 thermal and out-of-equilibrium processes.

25 **Introduction**

26

27 It is well established that cellular processes are intrinsically stochastic and therefore prone to
28 fluctuations [1-3]. The best-characterized examples of cellular noise relate to the variability in
29 expression of genes or proteins, observed either across a population of genetically identical cells
30 or within one cell over time [4, 5]. The molecular origins and physiological effects of such
31 expression noise are comparatively well understood [2-4, 6-8]. In contrast, noise that arises in
32 cellular networks at the posttranslational level remains much less characterized. Although such
33 noise is expected to be ubiquitous, e.g., in signaling networks, it was mostly observed indirectly
34 through its effects on gene expression or cell behavior [1, 3].

35 Chemotaxis of *Escherichia coli*, a bacterial model for signal transduction, previously provided
36 one example where signaling noise has been predicted based on analyses of cell motility and
37 flagellar rotation [9-15]. *E. coli* swims by a succession of straight runs during which the
38 bacterium advances, that are interrupted by short reorientations, or tumbles, which results in a
39 random walk. In chemical gradients, this random walk becomes biased by lengthening the runs
40 towards more favorable conditions. The chemotaxis pathway controlling this behavior is
41 composed of two modules, one mediating signal transduction and another adaptation, that
42 operate on different time scales [16-18] (Figure 1 – Figure Supplement 1A). The signal
43 transduction module includes sensory complexes consisting of the dimers of transmembrane
44 receptors, the kinase CheA and the scaffold protein CheW. Signaling by these complexes can be
45 understood in terms of a two-state model: In the absence of stimulation, receptor dimers are at
46 equilibrium between the active (ON) and inactive (OFF) states, resulting in an intermediate level
47 of autophosphorylation activity of the receptor-associated CheA. Positive chemotactic stimuli

48 (attractants) shift the equilibrium towards the OFF state, thus inhibiting CheA, whereas repellent
49 stimulation has the opposite effect. Downstream signal transduction occurs via phosphorylation
50 of the response regulator CheY that can subsequently bind to the flagellar motors to induce
51 tumbles. CheY is dephosphorylated with the help of the phosphatase CheZ. All reactions within
52 the signal transduction module occur within a few hundred milliseconds [19], ensuring that
53 swimming bacteria can faithfully monitor their current local environment.

54 The adaptation module operates on a much longer time scale of seconds to minutes. It includes
55 two enzymes, the methyltransferase CheR and the methylesterase CheB, which add or remove
56 respectively methyl groups at four specific glutamyl residues of the chemoreceptors. Since
57 receptor methylation increases the activity of the chemosensory complexes, these changes
58 gradually compensate for the effects of both attractant and repellent stimulation via a negative
59 feedback loop [20-22]. This enables bacteria to robustly maintain an intermediate steady-state
60 activity of CheA, and thus the level of CheY phosphorylation and frequency of cell tumbles,
61 even in the presence of steady background stimulation. Notably, in both major *E. coli*
62 chemoreceptors Tar and Tsr, two of the four methylated residues are initially encoded as
63 glutamines, *e.g.* Tar is expressed as Tar^{QEQE}. Glutamines are functionally similar to methylated
64 glutamates [23-26], and they are subsequently deamidated to glutamates by CheB [27, 28].

65 Despite this importance of the adaptation system for robust maintenance of the average signaling
66 output, it was suggested that the relatively small number of methylation enzymes [29] and their
67 slow exchange rates at their receptor substrates [30, 31] lead to fluctuations of the level of
68 phosphorylated CheY [9, 10, 12, 32, 33]. Further amplified by the cooperative response of the
69 flagellar motor [32, 34], these fluctuations were proposed to explain the observed large variation
70 in the motor rotation [9, 10, 15] and in the swimming behavior [9, 11, 13, 35] of individual cells

71 over time. Subsequent theoretical analyses suggested that such behavioral fluctuations might
72 provide physiological benefit, by enhancing environmental exploration [10, 36-40].

73 Another distinctive feature of the bacterial chemotaxis pathway is the clustering of
74 chemoreceptors in large signaling arrays, formed through a complex network of interactions
75 between trimers of receptor dimers, CheA and CheW [16]. Although signaling arrays are stable
76 on the time scale of signal transduction [31, 41], they appear to locally reorganize within minutes
77 [42]. Within arrays, the activity states of neighboring receptors are coupled, resulting in
78 amplification and integration of chemotactic signals [24, 25, 43-48]. These allosteric receptor
79 interactions have been previously described using either the Monod-Wyman-Changeux (MWC)
80 model [47] which assumes that receptors operate in units (signaling teams) of 10-20 dimers
81 where activities of individual receptors are tightly coupled [24, 46-49] or using an Ising model of
82 a receptor lattice with intermediate coupling [45, 46]. In both models, the sensitivity of signaling
83 arrays is highest at intermediate levels of receptor activity where receptors can easily switch
84 between ON and OFF states, with optimal intermediate activity being maintained by the
85 adaptation system [43, 44]. Another connection between the adaptation system and receptor
86 clustering is through adaptation assistance neighborhoods, where adaptation enzymes that are
87 transiently tethered to one receptor molecule can methylate (or demethylate) multiple
88 neighboring receptors [30].

89 In this work we directly quantify signaling noise in *E. coli* chemotaxis, using Förster
90 (fluorescence) resonance energy transfer (FRET) to monitor pathway activity in single cells and
91 with high time resolution. We show that the pathway activity fluctuations arise from interplay of
92 multiple factors, including not only the stochasticity of the methylation system but also
93 cooperative interactions and slow rearrangements of receptors within clusters. Finally, using

94 analysis based on the fluctuation-dissipation theorem (FDT) we could distinguish between
95 equilibrium and out-of-equilibrium fluctuations within the chemotaxis network and elucidate
96 respective contributions of receptor clusters and methylation to the overall noise.

97

98

99 **Results**

100

101 **Fluctuations of chemotaxis pathway activity in single cells**

102 To perform time-resolved measurements of the chemotaxis pathway activity in individual *E. coli*
103 cells, we adapted the microscopy-based ratiometric FRET assay [50] that relies on the
104 phosphorylation-dependent interaction between CheY, fused to yellow fluorescent protein
105 (CheY-YFP), and its phosphatase CheZ, fused to cyan fluorescent protein (CheZ-CFP) (Figure 1
106 – Figure Supplement 1A). The amount of this complex, and thus the level of FRET, provides a
107 direct intracellular readout of CheA activity [26, 50-52]. In previous studies where this assay was
108 applied to investigate chemotactic signaling in *E. coli* populations [18, 24, 26, 42, 44, 50-60],
109 bacteria expressing the FRET pair were immobilized in a flow chamber and fluorescent signals
110 were collected using photon counters from an area containing several hundred cells [50]. Here,
111 we used a similar setup but instead imaged fluorescence of the FRET pair with an electron
112 multiplication charge-coupled device (EM-CCD) camera (see Materials and methods and Figure
113 1 – Figure Supplement 1B, C).

114 As done previously [24, 26, 52, 55], we analyzed *E. coli* cells that express the CheY-YFP/CheZ-
115 CFP FRET pair instead of the native CheY and CheZ and have Tar as the only chemoreceptor
116 (see Materials and methods). The level of Tar expression in these cells and under our conditions

117 is $\sim 10^4$ dimers per cell [24, 26], comparable to the total level of endogenous chemoreceptors
118 [29]. When integrated over the population, the chemotactic response of these cells measured
119 using EM-CCD (Figure 1A and Figure 1 – Figure Supplement 2, upper panel) was very similar
120 to the one observed previously using area detectors [51, 55]. When bacteria in the flow chamber
121 were stimulated with the Tar-specific chemoattractant α -methyl-DL-aspartate (MeAsp), the ratio
122 of the YFP to CFP fluorescence (FRET ratio, $R(t) = YFP(t)/CFP(t)$) first rapidly decreased.
123 This is consistent with the fast attractant-mediated inhibition of the kinase activity, which results
124 in decreased formation of the FRET complex, and therefore reduced energy transfer from the
125 donor (CFP) to the acceptor (YFP) fluorophore. As 10 μ M MeAsp is known to fully inhibit the
126 kinase activity in this strain [24, 26], the value of the FRET ratio immediately after stimulation
127 reflects the zero activity baseline. Subsequently, the pathway adapted to the new background
128 level of attractant via the CheR-dependent increase in receptor methylation. But as previously
129 reported adaptation of Tar-only cells to high levels of MeAsp was only partial [53-55], meaning
130 that the adapted pathway activity remained lower than in buffer. Subsequent removal of
131 attractant resulted in a transient increase in kinase activity, followed by the CheB-mediated
132 adaptation through the demethylation of receptors.

133 Although the FRET ratio measured for individual cells during the same experiment was
134 expectedly noisier than the population-averaged data, both the initial response and subsequent
135 adaptation were clearly distinguishable (Figure 1A and Figure 1 – Figure Supplement 2, lower
136 panel). In contrast to the population measurement, however, a majority of individual cells also
137 exhibited large fluctuations in the FRET ratio on the time scale of 10-100 sec. For cells adapted
138 in buffer, the amplitude of these fluctuations could be as large as the response to strong attractant
139 stimulus. Confirming that this low-frequency noise reflects fluctuations of the pathway activity,

140 it was not observed when imaging either fluorescent beads or the same FRET pair in receptorless
141 cells that do not activate CheA (Figure 1 – Figure Supplement 3 A, B). Furthermore, inhibition
142 of the pathway activity by saturating stimulation with 10 μ M or 25 μ M MeAsp also transiently
143 suppressed long-term fluctuations, which subsequently (partly) reappeared upon (partial)
144 recovery of the pathway activity due to adaptation (Figure 1A and Figure 1 – Figure Supplement
145 2). In contrast, the higher-frequency noise in the FRET ratio could be observed in all strains and
146 conditions, including receptorless cells, indicating that it represents the noise of the
147 measurement. High-frequency noise was also observed in the control measurements using
148 fluorescent beads, although its magnitude was lower, consistent with higher brightness of beads
149 compared to the YFP/CFP expressing cells.

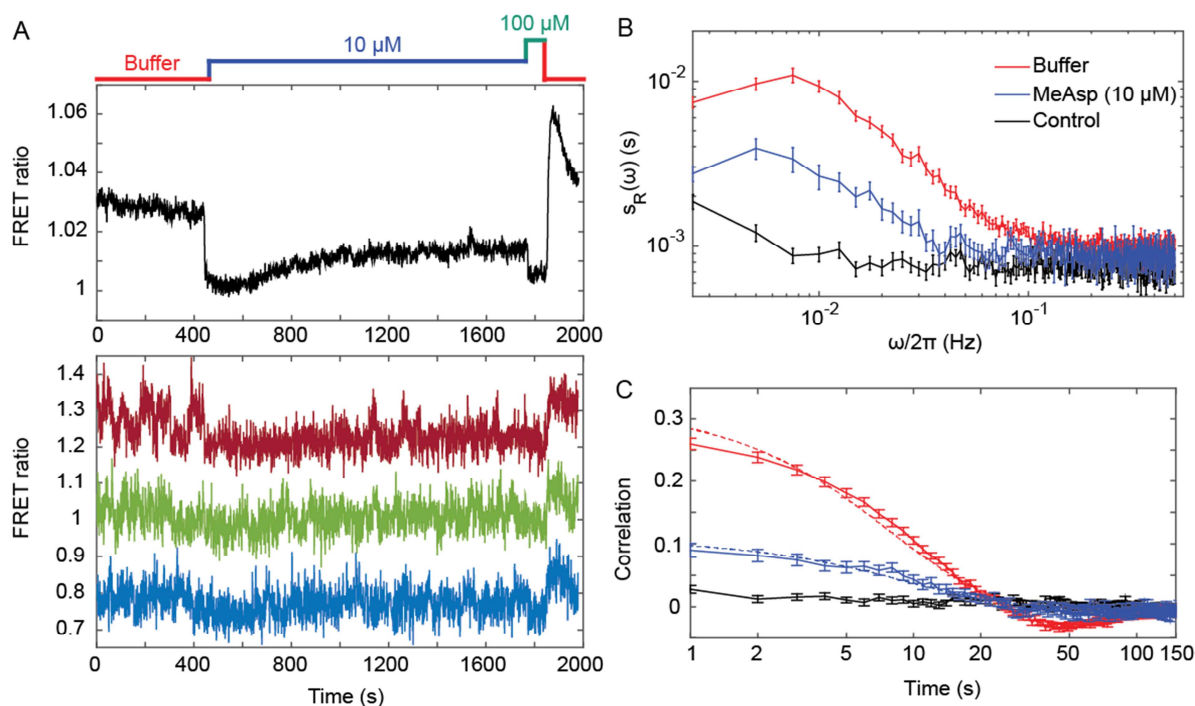
150 To analyze these activity fluctuations in greater detail, we computed the power spectral density
151 (PSD) of the single-cell FRET ratio, $s_R(\omega)$ (see Materials and methods). The PSD extracts the
152 average spectral content of the temporal variations of the single-cell FRET ratio, *i.e.* determines
153 the frequencies at which this ratio fluctuates, with $s_R(\omega)$ representing the magnitude of
154 fluctuations at a given frequency ω . We observed that at high frequency ($\omega > 0.1$ Hz) the PSD
155 kept a constant frequency-independent low value that was similar in all strains (Figure 1B). We
156 thus conclude that the noise in the FRET ratio in this frequency range is dominated by the shot
157 noise of the measurement. At lower frequency, however, the PSD measured for the Tar-
158 expressing cells adapted in buffer increased dramatically (roughly as $1/\omega$), reaching a low
159 frequency plateau at $\omega/2\pi \simeq 0.015$ Hz. A similar result was obtained for cells expressing Tar in
160 the unmodified (Tar^{EEEE}) state, where all glutamates are directly available for methylation by
161 CheR (Figure 1 – Figure Supplement 4A). The increase of the PSD at low frequency was also
162 observed for cells adapted to either 10 or 25 μ M MeAsp (Figure 1B and Figure 1 – Figure

163 Supplement 4A), although the amplitude of this increase was smaller than for the buffer-adapted
164 cells, apparently consistent with their lower pathway activity (Figure 1A and Figure 1 – Figure
165 Supplement 2). The receptorless strain showed nearly constant noise level over the entire
166 frequency range, as expected for white shot noise, although the PSD increased weakly at the
167 lowest frequency. As such increase was not observed for the control using fluorescent beads
168 (Figure 1 – Figure Supplement 3 A), it might be due to the slow drift of the FRET ratio arising as
169 a consequence of the slightly different bleaching rates of CFP and YFP, but possibly also to slow
170 changes in cell physiology. In any case, the contribution of this low-frequency component to the
171 overall PSD of the Tar-expressing cells is only marginal (note the log scale in Figure 1B), and
172 subtracting it did not markedly change our results (Figure 1 – Figure Supplement 5).

173 The PSD was further used to calculate the average time autocorrelation function of the single-
174 cell FRET ratio, which reflects the characteristic time scale of activity fluctuations (see Materials
175 and methods). For cells adapted in buffer, the autocorrelation time constant was 9.5 ± 0.5 s, as
176 determined by an exponential fit to the autocorrelation function (Figure 1D). This value is
177 similar to the characteristic time of the pathway activity fluctuation previously deduced from
178 behavioral studies [9, 14]. The same characteristic time was observed in MeAsp-adapted cells,
179 although the amplitude of the correlation was considerably smaller in this case (Figure 1D and
180 Figure 1 – Figure Supplement 4B). Interestingly, at longer times the autocorrelation function
181 becomes weakly negative, indicating an overshoot that is likely caused by the negative feedback
182 in the adaptation system [61]. As expected, no autocorrelation was observed for the receptorless
183 cells.

184 Finally, the variance of activity was evaluated from the PSD using Parseval's formula [62]. After
185 subtracting the variance measured for the receptorless strain, which reflects the contribution of

186 the shot noise, the specific variance of the FRET ratio for cells adapted in buffer was $\langle \Delta R^2 \rangle^+ =$
 187 0.0046 ± 0.0002 (where “+” refers to the presence of adaptation enzymes, $\text{CheR}^+ \text{CheB}^+$). As
 188 shown previously [50], the FRET ratio R is related to the relative pathway activity $\langle A \rangle$ as $R =$
 189 $\lambda \langle A \rangle + \mu$, where λ is the conversion factor and μ is a constant corresponding to the baseline
 190 FRET ratio at zero pathway activity (i.e., upon stimulation with saturating attractant
 191 concentration; Figure 1A). The value $\lambda = 0.10 \pm 0.01$ could be estimated as the mean difference
 192 between the measured FRET ratio values corresponding to the fully active (i.e., $\langle A \rangle = 1$) and
 193 fully inactive (i.e., $\langle A \rangle = 0$) pathway (see Materials and methods). The calculated variance of the
 194 pathway activity was $\langle \Delta A^2 \rangle^+ = 0.46 \pm 0.04$, indicating concerted activity fluctuations across
 195 much of the signaling array.
 196



197
 198 **Figure 1. Fluctuations of the chemotaxis pathway activity in individual $\text{CheR}^+ \text{CheB}^+$ cells.** (A) Time course of
 199 the FRET measurements for the $\text{CheR}^+ \text{CheB}^+$ strain expressing the FRET pair CheY-YFP and CheZ-CFP and Tar

200 as the sole receptor (see Materials and methods for details of expression), for cell population (upper panel) and for
201 representative single cells (lower panel). Cells immobilized in a flow chamber under steady flow (see Materials and
202 methods and Figure 1 – Figure Supplement 1B) were initially adapted in buffer (red) and subsequently stimulated by
203 addition and subsequent removal of indicated concentrations of a non-metabolizable chemoattractant MeAsp (blue
204 and green). The measurement traces for single cells have been shifted along the y-axis to facilitate visualization. (B)
205 Power spectral density (PSD) of the FRET ratio for single cells adapted in buffer (red curve) or in 10 μ M MeAsp
206 (blue curve), as well as for the control receptorless strain in buffer (black curve). (C) The corresponding time
207 autocorrelation functions of the single-cell FRET ratio. Dashed lines show fits by exponential decay (see Materials
208 and methods). The error bars represent standard errors of the mean (SEM), and the sample sizes are 265 (buffer), 69
209 (10 μ M) and 103 (receptorless control) single cells coming from at least three independent experiments in each case.

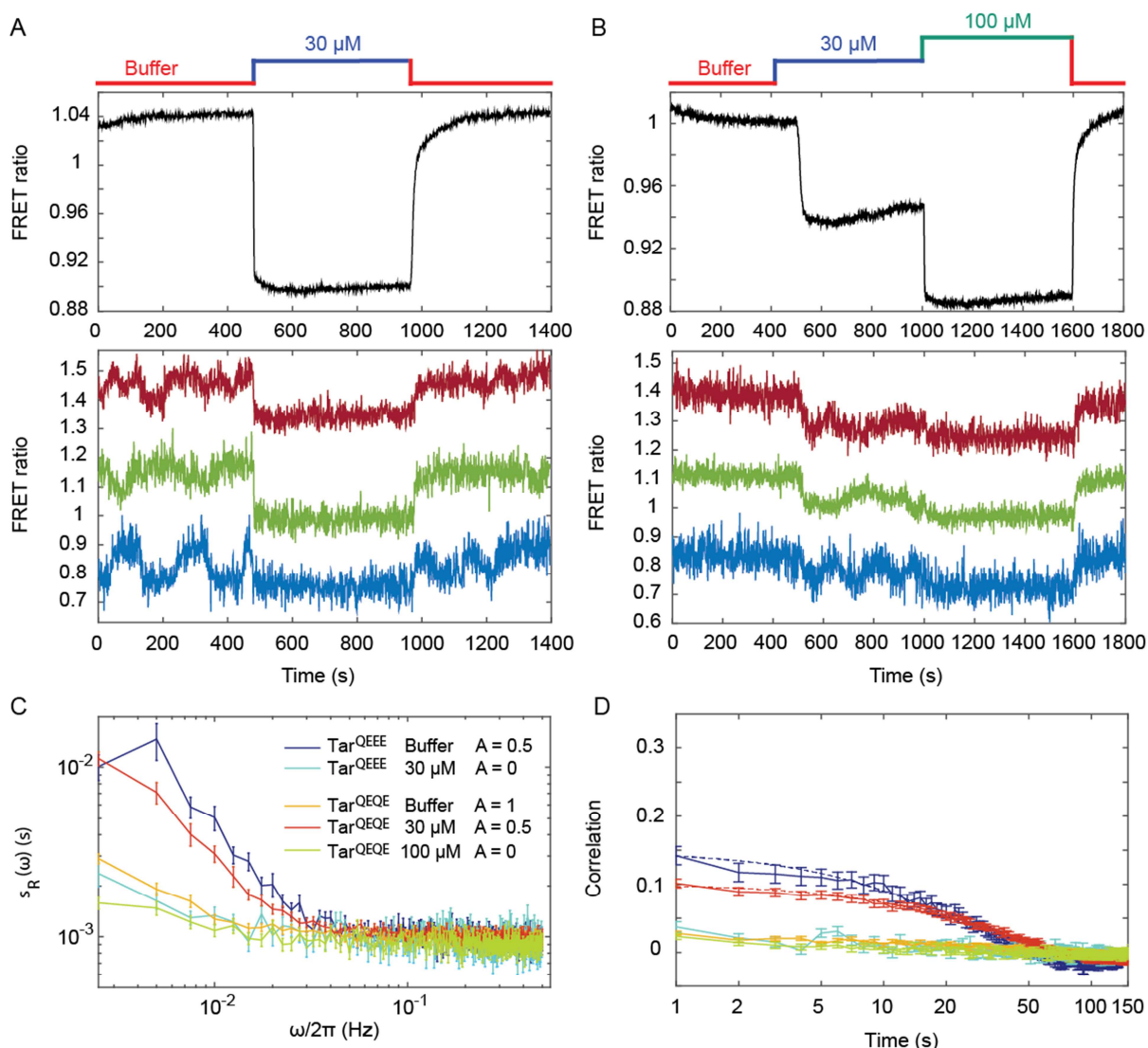
210

211 **Activity fluctuations in absence of adaptation system**

212 We next monitored the single-cell pathway activity in a strain lacking CheR and CheB, to test
213 whether the observed fluctuations could be solely explained by the action of the adaptation
214 system. Given the observed dependence of the fluctuations on the level of pathway activity, we
215 first analyzed a $\Delta cheR\Delta cheB$ strain that was engineered to express Tar receptor in one-modified
216 state (Tar^{QEEE}). This closely mimics the average modification state and intermediate activity of
217 Tar in CheR⁺ CheB⁺ cells adapted in buffer [26, 51]. Expectedly, $\Delta cheR\Delta cheB$ Tar^{QEEE} cells
218 responded to MeAsp but showed no adaptation comparable to CheR⁺ CheB⁺ cells (Figure 2A).
219 But despite the lack of the adaptation system, pathway activity in individual $\Delta cheR\Delta cheB$
220 Tar^{QEEE} cells showed pronounced long-term fluctuations when cells were equilibrated in buffer
221 (Figure 2A, lower panel). These methylation-independent long-term fluctuations were
222 suppressed upon saturating pathway inhibition with 30 μ M MeAsp, leaving only the shot noise
223 of the measurement.

224 In contrast to Tar^{QEEE} , $\Delta\text{cheR}\Delta\text{cheB}$ cells expressing the half-modified Tar^{QEQE} as the sole
225 receptor showed no long-term activity fluctuations in buffer (Figure 2B). Because Tar^{QEQE} is
226 known to be highly active (*i.e.*, strongly biased towards the ON state) in absence of attractants
227 [26, 52] and therefore insensitive to stimulation, we lowered its activity to an intermediate value
228 by stimulating cells with 30 μM MeAsp (Figure 2B, upper panel). This partial stimulation indeed
229 restored low-frequency fluctuations in $\Delta\text{cheR}\Delta\text{cheB}$ Tar^{QEQE} cells (Figure 2B, lower panel).
230 Again, these activity fluctuations were completely abolished upon saturating attractant
231 stimulation. Cumulatively, these results clearly demonstrate that, at intermediate level of activity
232 where the receptors are highly sensitive, pathway output fluctuates even in the absence of the
233 methylation system. These fluctuations were clearly identifiable above shot noise in the PSD of
234 the FRET ratio (Figure 2C), and they were absent under conditions of very low or very high
235 activity. Notably, these methylation-independent fluctuations were slower than those observed in
236 $\text{CheR}^+ \text{CheB}^+$ cells (Figure 2 – Figure Supplement 2), with a typical time scale of 34 ± 4 s, as
237 determined by fitting the time autocorrelation functions with an exponential decay (Figure 2D),
238 although this time might be slightly under-evaluated since it is already comparable to the total
239 duration of acquisition (400 s). Their amplitude, evaluated again using Parseval's formula, was
240 $\langle \Delta R^2 \rangle^- = 0.0025 \pm 0.0001$, corresponding to $\langle \Delta A^2 \rangle^- = 0.25 \pm 0.01$, and thus roughly half
241 of the amplitude of fluctuations observed in $\text{CheR}^+ \text{CheB}^+$ cells.

242



243

244 **Figure 2. Pathway activity fluctuations in $\Delta cheR\Delta cheB$ cells.** (A) Time course of population-averaged (black;

245 upper panel) and typical single-cell (colors; lower panel) measurements of the FRET ratio for $\Delta cheR\Delta cheB$ strain

246 expressing Tar^{QEEE} as the sole receptor. Measurements were performed as in Figure 1. Cells were first equilibrated

247 in buffer (red) and subsequently stimulated by addition (blue) and subsequent removal of 30 μM MeAsp, saturating

248 stimulus for this receptor. (B) Same as (A) but for $\Delta cheR\Delta cheB$ strain expressing Tar^{QEQE} as the sole receptor and

249 upon stimulation with 30 μM (blue) and then 100 μM (green) MeAsp. Note that for this receptor, 30 μM MeAsp is

250 the sub-saturating stimulus whereas 100 μM MeAsp is the saturating stimulus. The measurement traces for single

251 cells in (A) and (B) have been shifted along the y-axis to facilitate visualization. (C) PSD of the single-cell FRET

252 ratio for Tar^{QEEE} in buffer (blue) or in 30 μM MeAsp (cyan), Tar^{QEQE} in buffer (orange), in 30 μM MeAsp (red) or in

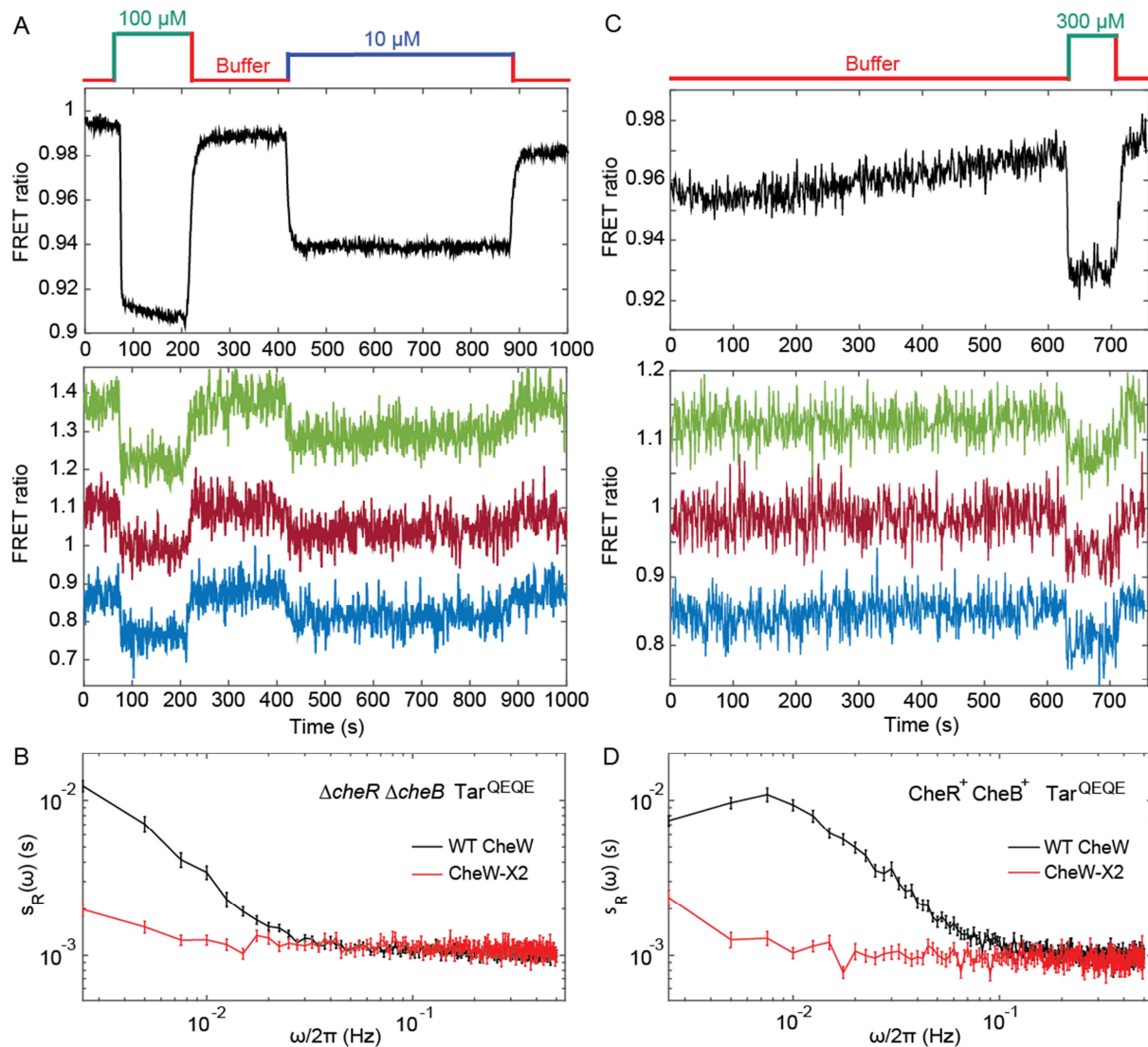
253 100 μ M MeAsp (yellow). (D) Corresponding time autocorrelation functions of the single-cell FRET ratio for
254 indicated strains/conditions. Dashed lines show fits by single exponential decay. Error bars represent standard errors
255 of the mean (SEM), and the sample sizes are 153 (Tar^{QEEE}, buffer), 65 (Tar^{QEEE}, 30 μ M), 471 (Tar^{QEQE}, buffer), 404
256 (Tar^{QEQE}, 30 μ M) and 136 (Tar^{QEQE}, 100 μ M) single cells coming from at least three independent experiments in
257 each case.

258

259 **Role of receptor clustering in signaling noise**

260 To investigate whether the observed fluctuations depend on clustering of chemotaxis receptors,
261 we utilized a recently described CheW-X2 version of the adaptor protein CheW that disrupts
262 formation of the receptor arrays without abolishing signaling [56]. This CheW mutant carries
263 two amino acid replacements, R117D and F122S, which are believed to break the receptor arrays
264 into smaller complexes consisting of two trimers of receptor dimers coupled to one CheA [44,
265 56]. The CheW-X2 is expressed at a level similar to the native CheW [44]. Consistent with
266 reported functionality of such complexes [44, 56, 63], a $\Delta cheR\Delta cheB$ strain expressing CheW-
267 X2 and Tar^{QEQE} showed basal activity and response to MeAsp which were similar to the
268 respective strain expressing the native CheW (Figure 3A and Figure 3 – Figure Supplement 1).
269 Nevertheless, this strain showed no apparent long-term fluctuations in the pathway activity
270 above the shot noise, even when its activity was tuned to an intermediate level by addition of 10
271 μ M MeAsp (Figure 3A,B). Similarly, the array disruption allowed signaling but abolished the
272 long-term activity fluctuations in CheR⁺ CheB⁺ cells equilibrated in buffer (Figure 3C,D).
273 Importantly, buffer-adapted CheR⁺ CheB⁺ CheW-X2 cells had intermediate receptor activity and
274 could respond to both attractant (MeAsp) and repellent (Ni²⁺) stimuli, *i.e.*, both down- and
275 upregulation of the pathway activity (Figure 3 – Figure Supplement 2). This confirms that the
276 observed loss of fluctuations was not caused by locking the receptor in the extreme activity state.

277 In summary, these results demonstrate that the observed long-term fluctuations in activity, seen
 278 both with and without the receptor methylation system, require receptor clustering.
 279



280
 281 **Figure 3. Fluctuation analysis in CheW-X2 cells.** (A) Population-averaged (upper panel) and typical single-cell
 282 (lower panel) measurements of the FRET ratio for $\Delta cheR\Delta cheB$ strain carrying CheW-X2 and Tar^{QEQE} as the sole
 283 receptor. Cells, which have a high activity in buffer, were first exposed to 100 μ M MeAsp (saturating stimulus), and
 284 then to 10 μ M MeAsp (sub-saturating stimulus), as indicated. The single-cell measurement traces have been shifted
 285 along the y-axis to facilitate visualization. (B) Power spectral density of the FRET ratio fluctuations in CheW-X2
 286 $\Delta cheR\Delta cheB$ Tar^{QEQE} cells at intermediate activity (i.e., with 10 μ M MeAsp) (red) compared to the equivalent strain

287 carrying native (wild-type; WT) CheW and at 30 μM MeAsp (black – same data as Figure 2C). Error bars represent
288 SEM, with sample sizes 404 (WT CheW; black) and 208 (CheW-X2; red) cells. (C) Same as (A) but for CheR⁺
289 CheB⁺ strain. The activity in buffer is at intermediate level (Figure 3 – Figure Supplement 2), with 300 μM MeAsp
290 completely inhibiting the kinase activity. (D) Power spectral density of the FRET ratio fluctuations in CheR⁺ CheB⁺
291 CheW-X2 strain in buffer (red) compared to the native WT CheW (black – same data as Figure 1C). Error bars
292 represent SEM, with sample sizes 265 (WT CheW; black) and 191 (CheW-X2; red) cells.

293

294 **Fluctuation-dissipation relation for receptor clusters**

295 We next used mathematical analysis to better understand the respective contributions of receptor
296 clustering and the methylation enzymes to the observed fluctuations and to determine whether
297 methylation-independent fluctuations are generated by some out-of-equilibrium random process.

298 We considered the fluctuation-dissipation theorem (FDT), which postulates – *for systems at*
299 *equilibrium* – that thermal fluctuations of a quantity are related, via temperature, to the response
300 of this quantity to a small externally applied perturbation [64]. The FDT framework can be used
301 to determine whether a system is at equilibrium, by comparing fluctuations and responses to
302 small perturbations *via* their ratio, the so-called effective temperature $T_{\text{eff}}(\omega)$ [65-68]. In
303 equilibrium systems the FDT is satisfied and $T_{\text{eff}}(\omega)$ equals the physical temperature T . In out-
304 of-equilibrium (biological) systems, the deviation of $T_{\text{eff}}(\omega)$ from T provides a first
305 characterization of the underlying out-of-equilibrium noisy process generating the fluctuations,
306 since $T_{\text{eff}}(\omega)$ is linked to the energy scale and frequency content of such process [65-68].

307 In our case, the magnitude of activity fluctuations could be expressed as the PSD corrected for
308 the measurement shot noise, $s_R(\omega) - \epsilon_n^2$, where ϵ_n^2 was experimentally determined as the PSD
309 of the receptorless cells. We therefore define the effective temperature as:

$$\frac{T}{T_{\text{eff}}(\omega)} = \frac{G_R(\omega)}{s_R(\omega) - \epsilon_n^2}. \quad (1)$$

310 The dissipation $G_R(\omega)$ could be determined by formulating the fluctuation dissipation relation
311 for the activity of individual receptors within the signaling array, using the Ising-like model [45,
312 69, 70] to describe cooperative receptor interactions as (see Appendix, section 1):

$$G_R(\omega) = -2 \lambda^2 \frac{3N^2 \langle A \rangle (1 - \langle A \rangle)}{N_T} \text{Re}(\hat{g}(\omega)). \quad (2)$$

313 Here $\langle A \rangle$ is the average activity around which fluctuations occur, estimated from experimental
314 data as described above, N_T is the total number of Tar dimers per cell, N is the average number
315 of effectively coupled allosteric signaling units in the cluster, and λ is defined as before.
316 Consistent with several recent reports [44, 56, 63] and with our analysis of the apparent response
317 cooperativity in the CheW-X2 strain (Figure 3 – Figure Supplement 1 and Appendix, section
318 1.4), we assumed that signaling units within the cluster correspond to trimers of receptor dimers.
319 Finally, $\text{Re}(\hat{g}(\omega))$ is the real part of the Fourier transform of the normalized step response
320 function $g(t)$, which could be experimentally determined by measuring the FRET response to
321 sufficiently small (subsaturating) stepwise attractant stimulation as $g(t) = \Delta R(t) / (-\lambda X_A^\infty \epsilon_0)$,
322 where $(-\lambda X_A^\infty \epsilon_0)$ is the normalized stimulation strength (see Appendix, section 1.3).

323 For subsaturating stimulation of the non-adapting $\Delta cheR \Delta cheB$ cells (Figure 2B), the normalized
324 step response function $g^-(t)$ exhibited a relatively rapid initial increase and then slowly
325 approached its final value, possibly with a slight transient overshoot (Figure 4A). Nearly
326 identical response dynamics was observed for weaker stimulations (Figure 4 – Figure
327 Supplement 1), validating the small perturbation assumption of the FDT for this response
328 function measurement. This slow response dynamics is consistent with a previous report that
329 attributed it to gradual stimulation-dependent changes in packing of receptors within clusters
330 [42]. Consistent with this interpretation, the CheW-X2 $\Delta cheR \Delta cheB$ strain with disrupted

331 receptor clustering showed neither comparable latency nor overshoot in its response (Figure 3 –
332 Figure Supplement 3).

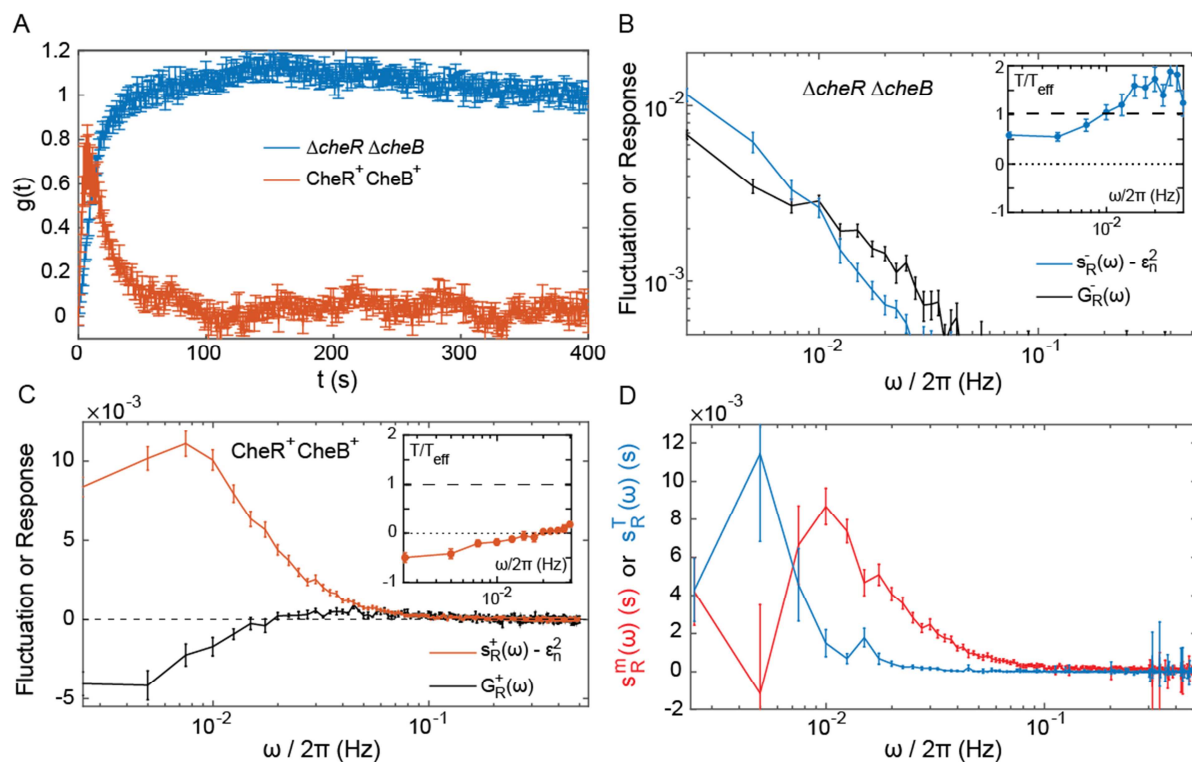
333 As the pathway activity in the CheW-X2 in $\Delta cheR\Delta cheB$ strain also showed no long-term
334 fluctuations (Figure 3B,C), we hypothesized that these fluctuations might be indeed caused by
335 the slow response dynamics stimulated by some random process. We thus calculated the
336 corresponding dissipation using Equation (2), considering that under our conditions $N_T \sim 10^4$
337 [26] and $N \sim 14$ [26, 53, 58, 60] (see Table 1 for all parameter values). At low frequencies, the
338 dissipation $G_R(\omega)$ was approximately equal to the shot-noise corrected $s_R(\omega)$ at $\langle A \rangle \simeq 0.5$
339 (Figure 4B), as predicted by Equation (1) for equilibrium systems where $T_{\text{eff}}(\omega)$ equals T .
340 Consistently, the corresponding ratio $T/T_{\text{eff}}(\omega)$ was nearly independent of ω and close to unity
341 in the range of frequencies for which $s_R(\omega)$ is above the measurement noise (Figure 4B *Inset*).
342 This suggested that in absence of adaptation enzymes the system is close to equilibrium and
343 thermal fluctuations are the major source of noise. Although the deviation of $T/T_{\text{eff}}(\omega)$ from
344 unity might indicate second-order contributions of out-of-equilibrium processes, it is comparable
345 to what was observed for other equilibrium systems with measurement methods of similar
346 precision [66, 71, 72]. Thus, an equilibrium model can fairly accurately describe the details of
347 observed long-time activity fluctuations in $\Delta cheR\Delta cheB$ cells. This agreement suggests that the
348 receptor cluster in these cells largely acts as a passive system, where thermal fluctuations
349 stimulate the long-term response dynamics, possibly due to slow changes in receptor packing
350 within clusters, to generate activity fluctuations.

351 Furthermore, the PSD of $\Delta cheR\Delta cheB$ cells followed the scaling $\langle A \rangle(1 - \langle A \rangle)$, which is
352 expected from the underlying receptor activity being a two-state variable, as evident for
353 subpopulations of cells sorted according to their activity (Figure 4 – Figure Supplement 2), with

354 which our FDT analysis is consistent (Equation (2)). Fluctuations were apparently unaffected by
355 the expression level of Tar, in the tested range of induction (Figure 4 – Figure Supplement 3). In
356 the FDT framework, this implies that N^2/N_T must be constant for varying receptor expression,
357 and previous measurements indeed suggest that the cooperativity rises with the expression level
358 of Tar^{QEQE} in a way that N^2/N_T remains unchanged [26].

359 To evaluate the respective effects of signal amplification and the slow dynamics of the cluster
360 activity response, we performed stochastic simulations of a simple model of sensory complexes
361 without adaptation and under thermal noise (see Appendix, section 4). In this model, receptors
362 are clustered in signaling teams that respond to allosterically amplified free energy changes on an
363 effective time scale averaging the fast switching dynamics and the slow dynamics of the receptor
364 cluster, which accounts qualitatively for the pathway behavior. Expectedly, larger amplification
365 led to larger fluctuations, and the time scale of the fluctuations followed the imposed response
366 time scale of the cluster. Less trivially, slower response also led to higher maximal amplitude of
367 the fluctuations (Figure 4 – Figure Supplement 4).

368



369
 370 **Figure 4. Fluctuation-dissipation analysis of the pathway activity.** (A) Step response function $g(t)$ both in
 371 presence (red) and in absence (blue) of the adaptation enzymes, evaluated in cells expressing Tar^{OEQE} that respond to
 372 a step change from buffer to $0.3 \mu\text{M}$ MeAsp ($\text{CheR}^+ \text{CheB}^+$) or $30 \mu\text{M}$ MeAsp ($\Delta\text{cheR}\Delta\text{cheB}$). The step response
 373 function was calculated from the measurements shown in Figure 4 – Figure Supplement 5 and in Figure 2B as
 374 described in text and in Appendix, section 1.3. (B,C) The PSD of the FRET ratio fluctuations $s_R(\omega)$ at $\langle A \rangle = 0.5$
 375 (blue in B and red in C), and the corresponding dissipation $G_R(\omega)$ (black) calculated using Equation (2), for
 376 $\Delta\text{cheR}\Delta\text{cheB}$ (B) and $\text{CheR}^+\text{CheB}^+$ (C) cells. The measurement shot noise ϵ_n^2 , determined as the PSD of the
 377 receptorless cells (Figure 1B), was subtracted from $s_R(\omega)$. *Insets* show the ratio between the physical and effective
 378 temperatures, calculated using Equation (1). Dashed and dotted lines in B and C indicate $T/T_{\text{eff}}(\omega) = 1$ and
 379 $T/T_{\text{eff}}(\omega) = 0$, respectively. (D) Contribution of thermal noise (blue) and the adaptation enzyme dynamics (red)
 380 to the PSD in $\text{CheR}^+\text{CheB}^+$ cells, calculated from Equation (3) as explained in Appendix, section 3. In all panels, error
 381 bars represent SEM, with sample sizes for the power spectra calculations being 540 ($\Delta\text{cheR}\Delta\text{cheB}$) and 468 (CheR^+
 382 CheB^+ ; aggregating data from cells expressing Tar^{OEQE} and Tar^{EEEE} as sole receptor) single cells from at least five
 383 biological replicates.

384

385 **Out-of-equilibrium dynamics in presence of adaptation system**

386 The normalized step response function of CheR⁺ CheB⁺ cells, $g^+(t)$ (Figure 4A), was
387 determined using weak stimulation by 0.3 μ M MeAsp, with the activity change $\Delta A/\langle A \rangle = 0.25$
388 (Figure 4 – Figure Supplement 5 and Appendix, section 1.3). Describing adaptation according to
389 the classical two-state models of receptors [20, 60, 73], the responses of $\Delta cheR\Delta cheB$ and CheR⁺
390 CheB⁺ cells could be linked via the rate of adaptation ω_{RB} , which yielded $\omega_{RB} = 0.06 \pm$
391 0.01 Hz (Appendix, section 2 and Figure 4 – Figure Supplement 6), consistent with previous
392 estimates [14].

393 The corresponding dissipation $G_R^+(\omega)$, calculated as above according to Equation (2), differed
394 strongly from the PSD of the activity fluctuations (Figure 4C), confirming that the system
395 operates out of equilibrium. The corresponding $T/T_{\text{eff}}(\omega) \ll 1$ (Figure 4D *Inset*) is consistent
396 with strong out-of-equilibrium drive. It decreased at low frequencies, crossing zero at $\omega/2\pi \simeq$
397 0.015 Hz where $T_{\text{eff}}(\omega)$ diverges (Figure 4 – Figure Supplement 7) and dissipation becomes
398 negative. Such crossing indicates a transition to the range of frequencies where the active process
399 dominates [66, 74], with the frequency of divergence of $T_{\text{eff}}(\omega)$ representing interplay between
400 the time scales of the passive receptor response and adaptation (Appendix, section 2.2).

401 To further separate specific contributions of the methylation system and thermally activated
402 receptor cluster rearrangements to the power spectrum of activity fluctuations in CheR⁺ CheB⁺
403 cells, we followed previous modeling approaches [75-77] (Appendix, section 3). Assuming that
404 thermal noise behaves the same in presence and in absence of the methylation system, $s_R^+(\omega)$ can
405 be decomposed into a “thermal” contribution $s_R^T(\omega)$ and a contribution of the methylation noise
406 $s_R^m(\omega)$:

$$s_R^\dagger(\omega) = s_R^m(\omega) + s_R^T(\omega) = s_R^m(\omega) + \left| \frac{g^+(\omega)}{g^-(\omega)} \right|^2 s_R^-(\omega). \quad (3)$$

407 Although relatively noisy, particularly at low frequencies, $s_R^m(\omega)$ inferred from equation (3)
408 peaked around $\omega_{peak}/2\pi = 0.01$ Hz (Figure 4D), which equals the independently determined
409 adaptation rate (see above), $\omega_{peak} \simeq \omega_{RB} = 0.06$ Hz. The contribution of the thermal noise
410 $s_R^T(\omega)$ had a similar magnitude but dominated at lower frequencies. The power spectrum of the
411 CheR and CheB binding events was inferred from $s_R^m(\omega)$ using the previous model and previous
412 conclusion that the methylation-dependent activity fluctuations mainly arise from the intermittent
413 binding of the small number of CheR and CheB molecules to the receptors [33]. This spectrum
414 was consistent with the common assumption that CheR (CheB) loads and acts only on the
415 inactive (active) receptor (Appendix, section 3 and Figure 4 – Figure Supplement 8).

416 We further extended our simulation model of the receptor array composed of independent
417 signaling teams, to test whether we can reproduce the observed power spectrum in presence of
418 adaptation enzymes. Consistent with the large excess of receptors compared to the methylation
419 enzymes [29], in these simulations only one CheR (or CheB) molecule can bind to the inactive
420 (respectively active) receptor team, methylate (respectively demethylate) the receptors, and
421 unbind once the team has turned active (respectively inactive) (Appendix, section 4). The
422 simulations agreed qualitatively well with the experiments, including the power spectra of
423 CheR/CheB binding and effective temperature (Figure 4 – Figure Supplement 9), although
424 absolute amplitudes of the fluctuations were clearly underestimated by the model, as already
425 observed in a previous theoretical work [74]. The simulation also reproduced the loss of slow
426 fluctuations upon disruption of clusters in CheR⁺ CheB⁺ cells, which arises from the dependence
427 of $s_R(\omega)$ on the size N of signaling teams. In contrast, simulating less efficient neighborhood

428 assistance by reducing the (de)methylation rate of the bound enzymes had only modest effects
429 (Figure 4 – Figure Supplement 9C).

430

431 **Discussion**

432

433 Stochastic activity fluctuations are likely to have major impact on signal processing within
434 cellular networks [1, 3]. Nevertheless, direct visualization and characterization of such
435 fluctuations at the posttranslational level remain limited to a small number of cases [78, 79]
436 primarily due to high requirements for the sensitivity and time resolution of the necessary single-
437 cell measurements. Although fluctuations of the signaling activity can in some cases be deduced
438 from the downstream output of the network, either gene expression [80, 81] or behavior [9, 10,
439 14, 33], this output may strongly filter and reshape fluctuations. Consequently, the theoretical
440 framework for the analysis of noise at the posttranslational level remains less developed than for
441 variations in gene expression [4, 6].

442 Here we directly monitored activity fluctuations in the chemotaxis pathway of *E. coli*, a common
443 model for quantitative analysis of signal transduction [43, 82, 83]. One fascinating feature of the
444 chemotaxis pathway is the amplification of chemotactic signals through cooperative interactions
445 within the clusters (arrays) of chemoreceptors, where at least ~10-20 receptor dimers show
446 concerted transitions between active and inactive states [24, 25, 45-48]. The pathway is also
447 robust against external and internal perturbations, largely thanks to its methylation-based
448 adaptation system [20, 52, 84-86]. At the same time, the stochastic activity of the adaptation
449 enzymes was also proposed as the reason for the observed strong variability in the signaling
450 output, *i.e.* the duration of straight runs of the swimming cells [9, 10, 33]. Indeed, inspired by so-

451 called fluctuation-response theorems, previous analyses established a fluctuation-response
452 relation between the adaptation time to stimuli (called response time) and the typical time scale
453 of fluctuations of the tumbling rate in individual *E. coli* cells [10, 14] – which we confirmed at
454 the level of CheY phosphorylation ($\omega_{peak} \simeq \omega_{RB}$) – demonstrating that behavioral fluctuations
455 originate within the chemotaxis pathway and pointing to the methylation system as their likely
456 cause. Subsequently, the fluctuations in straight run durations were proposed to enhance
457 environmental exploration, partly since the occasional long run allows exploring wider territories
458 [10, 15, 37, 39, 40].

459 Here we combined experimental and mathematical analyses to demonstrate that both, the
460 adaptation system and receptor clustering contribute to the signaling noise in the chemotaxis
461 pathway. Experimentally, we adapted the FRET-based assay that was previously applied to study
462 average signaling properties in cell populations [18, 24, 26, 42, 44, 50-60], to be used at the
463 single-cell level. Whereas previous studies have relied on the output provided by flagellar motor
464 rotation [9, 14], using FRET enabled us to characterize the activity fluctuations directly, before
465 their amplification by the motor. Our measurements showed that fluctuations can be comparable
466 to the average adapted activity of the pathway and thus significantly larger than previous
467 estimates [32]. This surprisingly large amplitude of fluctuations indicates concerted variations of
468 receptor activity across the signaling arrays containing hundreds to thousands of receptors.
469 Furthermore, we showed that the stochasticity of receptor methylation could not be the sole
470 cause of the pathway noise, because activity fluctuations were also observed in absence of the
471 methylation system. In contrast, disruption of receptor clustering completely abolished these
472 long-term activity fluctuations, even in presence of the methylation system, implying that
473 receptor interactions are essential for the observed fluctuations.

474 To better understand the nature of the observed fluctuations, we applied analysis based on the
475 fluctuation-dissipation theorem (FDT), following a recent theoretical study [74]. The FDT
476 establishes a fundamental relationship between thermal fluctuations and the response to
477 externally applied perturbations for an equilibrium system. Although being a powerful tool for
478 studying equilibrium and out-of-equilibrium systems in physics [64], so far it has found only
479 limited application in biology [6, 65, 67, 87, 88]. For the chemotaxis system, the FDT in its
480 equilibrium form was used to predict the magnitude of thermally activated ligand binding noise
481 with implications for maximal sensing accuracy [77, 88]. The present approach is also
482 complementary to the previous fluctuation-response analysis mentioned above [10, 14], itself
483 conceptually related to the fluctuation theorems extending the FDT for certain systems in non-
484 equilibrium steady states [14, 89]. Comparison of fluctuations and dissipation to evaluate
485 whether the system deviates from the FDT, together with the analysis of mutants deficient in
486 adaptation and/or clustering, enabled to identify multiple factors contributing to the pathway
487 noise. These factors include (i) the input thermal noise, (ii) the amplification of this noise by
488 cooperative interactions among receptors, (iii) the delayed response function of receptor clusters,
489 and (iv) the dynamics of the methylation system (Figure 5).

490 Unexpectedly, the activity fluctuations in absence of the adaptation system could be explained
491 for the most part by thermal noise acting on the receptors, which is amplified through the
492 cooperative interactions of clustered receptors and subsequently converted into long-term
493 pathway activity fluctuations by their slow response dynamics (Figure 5A). The contribution of
494 out-of-equilibrium processes to these activity fluctuations seems to be minor if any. This
495 phenomenon demonstrates that thermal noise can induce measurable fluctuations in activity of a
496 cellular network, even in absence of active processes that are usually considered to be the main

497 contributors to cellular dynamics. Even more striking is the amplitude of these fluctuations,
498 suggesting that up to a half of the chemoreceptor array – that may contain thousands of receptors
499 – flips its activity.

500 The slow cluster dynamics was recently observed using fluorescence anisotropy measurements
501 and attributed to the stimulation-induced changes in packing of receptors within clusters [42].
502 Indeed, in our experiments both slow response and activity fluctuations were abolished by
503 mutations that disrupt clustering, suggesting that it corresponds to some large-scale plasticity
504 within the receptor array [44]. Interestingly, such stimulation-induced slow reconfiguration had
505 been also proposed to modulate cooperativity within the receptor array in an earlier theoretical
506 study [69]. Although the precise mechanism behind this slow dynamics was not yet
507 characterized, meaning that it could neither be experimentally disentangled from signal
508 amplification nor mechanistically modeled, our simulations suggest that while slow dynamics
509 sets the time scale of activity fluctuations, both this dynamics and amplification contribute to
510 their amplitude. It thus seems that this previously little considered feature of the receptor array
511 plays a large role in producing and shaping the activity fluctuations.

512 Our analysis also suggests that an effective subunit of the allosteric signaling teams corresponds
513 to one trimer of dimers, rather than a dimer itself as assumed in previous computational models
514 [26, 73]. This conclusion is consistent with several recent studies [44, 56, 63], and it could be
515 easily reconciled with the previous formulations of the Monod-Wyman-Changeux models by
516 rescaling the free-energy change per methylated glutamate by a factor of three. Since large size
517 of the cooperative units implies fewer units per receptor array, it further helps to account for the
518 large activity fluctuations even in absence of the methylation enzymes.

519 Notably, on the studied range of time scales the previously proposed contribution of the high-
520 frequency ligand binding noise [77, 88] to overall fluctuations must be very small, since the
521 observed power spectral densities depended on activity but not on the absolute ligand
522 concentration. The dynamics of CheY/CheZ interaction is also unlikely to contribute to the
523 observed fluctuations because the turnover rate of this complex (> 1 Hz) [29, 52] is above the
524 frequency range of our experiments.

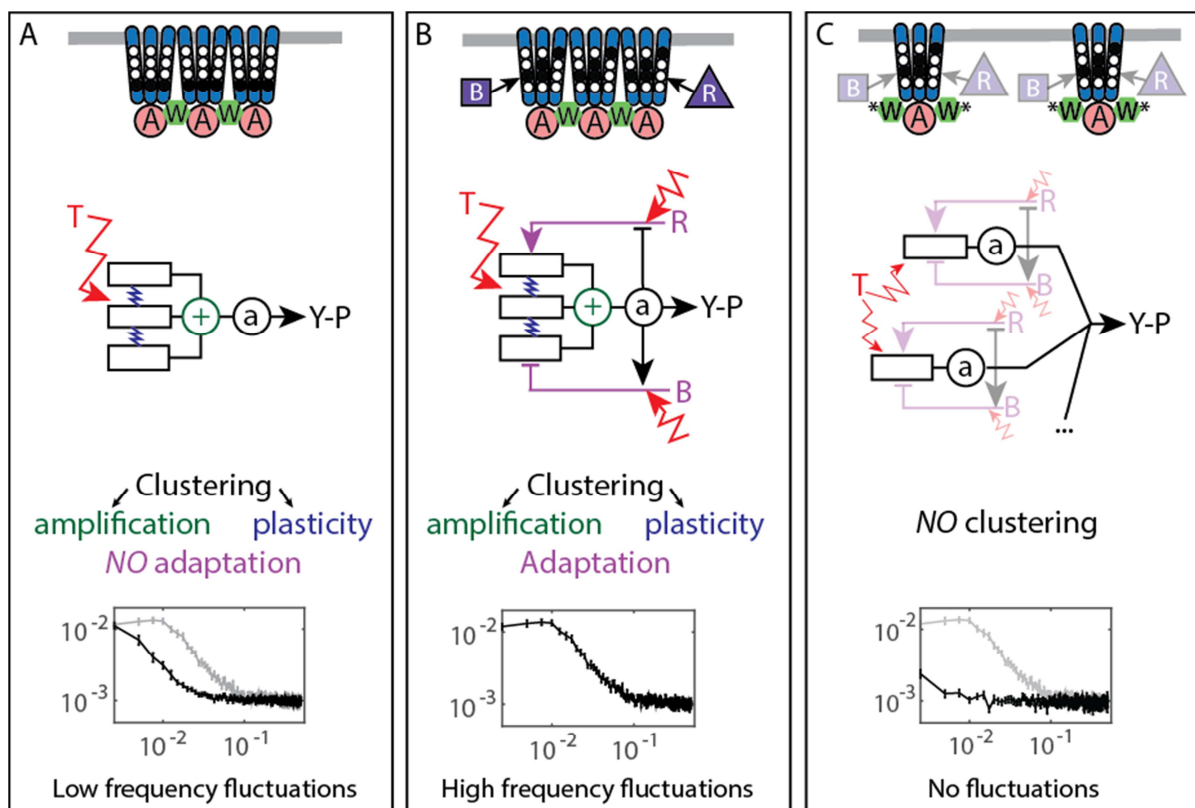
525 In the presence of the adaptation system the noise within receptor arrays is apparently added to
526 the noise coming from the stochasticity of methylation events (Figure 5B), with both noise
527 sources having comparable strength. The adaptation system not only shifts the frequency
528 spectrum of fluctuations but also eliminates the latency of the response to stimuli, thus likely
529 accelerating the response through its negative feedback activity. The statistics of methylation
530 events inferred from the power spectra was compatible with previous understanding of the
531 enzyme kinetics, including the hypothesis that methylation noise is enhanced by the
532 ultrasensitivity to changes in the ratio of methylation enzymes [9, 10]. Nevertheless, receptor
533 clustering is required for the observed activity fluctuations even in presence of the adaptation
534 system (Figure 5C), likely because of signal amplification as well as accelerated adaptation
535 dynamics within clusters due notably to assistance neighborhoods [30, 33, 56]. Our simulations
536 suggested that the former likely plays a more prominent role in generating large activity
537 fluctuations.

538 Altogether, the overall picture of the signaling noise in the chemotaxis pathway is more complex
539 than previously suggested, with the noise being first processed through a slow responding
540 amplifier (the chemoreceptor cluster) and then fed back through the methylation system,

541 resulting in complex colored fluctuations of the pathway activity and therefore of the swimming
542 behavior.

543 More generally, our study provides another example of the general relation between fluctuations
544 and response in biological systems and it demonstrates that FDT-based analysis can distinguish
545 between active and passive processes also within an intracellular network. Although activity
546 fluctuations in biological systems are commonly shaped by active, out-of-equilibrium processes,
547 meaning that in many cases the FDT will not be satisfied [14], the properties of a system can
548 nevertheless be inferred when studying the deviation of its behavior from the FDT [65-67, 87].
549 The approach of quantifying such deviations by means of an effective temperature, or
550 fluctuation-dissipation ratio, has been used in a variety of out-of-equilibrium systems [68], from
551 glasses to biological systems. Although in some systems, *e.g.* glasses, this ratio can have indeed
552 properties normally associated with the thermodynamic temperature, in biological systems the
553 effective temperature rather relates to the energy scale and frequency content of the underlying
554 out-of-equilibrium processes. This relation was previously demonstrated for several systems,
555 including the hair bundle of the inner ear [66] and active transport in eukaryotic cells [65, 67,
556 87], and we show that it also applies to a signaling pathway. Notably, the present analysis differs
557 both in its aims and technicalities from the aforementioned fluctuation-response analysis [10,
558 14]. For instance, the FDT breakdown in $\text{CheR}^+\text{CheB}^+$ cells does not contradict the previously
559 observed relation between fluctuation and adaptation time scales, since these two observations
560 provide different information: that the noise source encompasses an out-of-equilibrium process
561 and that the fluctuations originate in the chemotaxis pathway, respectively. An interesting
562 emergent feature of our analysis is the negative effective temperature, which arises as a hallmark
563 of the delayed adaptive negative feedback [74]. A similar effect was also observed in inner ear

564 hair bundles, where it is related to the mechanical adaptation feedback [66]. Negative dissipation
 565 associated to the negative temperature was predicted to indicate a reversal of causality, induced
 566 here by adaptation [74]: Whereas positive dissipation means that changes in receptor free energy
 567 induce activity changes, negative dissipation results from the methylation system counteracting
 568 preceding activity changes [74, 76, 90] and actively translating them into free energy changes,
 569 thus opposing the passive behavior of the receptors. Importantly, because the FDT-based
 570 analysis requires only knowledge of system's fluctuations and its response, it is widely
 571 applicable for studying dynamics of diverse cell signaling processes, including those where
 572 molecular details are not known.



573
 574 **Figure 5. Multiple sources of signaling fluctuation in the chemotaxis pathway.** (A) In the absence of adaptation
 575 enzymes, thermal fluctuations stimulating – and amplified by – the dynamic receptor cluster lead to low frequency
 576 fluctuations (<math>< 0.01 \text{ Hz}</math>) around intermediate cluster activity. The blue springs symbolize the plasticity of the receptor

577 array, the green \oplus its cooperativity. (B) In adapted wild-type cells, thermal fluctuations and fluctuations in the
578 dynamics of CheR and CheB are amplified by the dynamic chemoreceptor cluster, which leads to fluctuations of the
579 activity at frequencies around 0.03 Hz. (C) In the absence of clustering, responsive but non-amplifying receptor
580 complexes do not produce observable activity fluctuations, whether or not adaptation enzymes are present. Graphs
581 show the PSD of the FRET ratio measured in each respective case (black). In (A,C) the wild-type curve is shown for
582 comparison (gray).

583

584 **Materials and methods**

585

586 **Cell growth, media and sample preparation**

587 *E. coli* strains and plasmids are listed in Supplementary file S1A and S1B, respectively. Cells
588 carrying two plasmids that encode respectively Tar in the indicated modification states and the
589 FRET pair were grown at 30°C overnight in tryptone broth (TB) supplemented with appropriate
590 antibiotics. The culture was subsequently diluted 17:1000 in TB containing antibiotics, 2 μ M
591 salicylate (unless otherwise stated) for induction of Tar and 200 μ M isopropyl β -D-1-
592 thiogalactopyranoside (IPTG) for induction of the FRET pair, and grown at 34°C under vigorous
593 shaking (275 rpm) to an $OD_{600} = 0.55$. Bacteria were harvested by centrifugation, washed thrice
594 in tethering buffer (10 mM KPO_4 , 0.1 mM EDTA, 1 μ M methionine, 10 mM lactic acid, pH 7)
595 and stored at least 20 minutes at 4°C prior to the experiments.

596

597 **Microscopy**

598 Bacterial cells were attached to poly-lysine coated slides which were subsequently fixed at the
599 bottom of a custom-made, air-tight flow chamber, which enables a constant flow of fresh
600 tethering buffer using a syringe pump (Pump 11 Elite, Harvard Apparatus, Holliston,

601 Massachusetts, United States) at 0.5 ml/min. This flow was further used to stimulate cells with
602 indicated concentrations of α -methyl-D,L-aspartate (MeAsp). The cells were observed at 40x
603 magnification (NA = 0.95) using an automated inverted microscope (Nikon Ti Eclipse, Nikon
604 Instruments, Tokyo, Japan) controlled by the NIS-Elements AR software (Nikon Instruments).
605 The cells were illuminated using a 436/20 nm filtered LED light (X-cite exacte, Lumen
606 Dynamics, Mississauga, Canada), and images were continuously recorded at a rate of 1 frame
607 per second in two spectral channels corresponding to CFP fluorescence (472/30 nm) and YFP
608 fluorescence (554/23 nm) using an optosplit (OptoSplit II, CAIRN Research, Faversham, United
609 Kingdom) and the Andor Ixon 897-X3 EM-CCD camera (Andor Technology, Belfast, UK) with
610 EM Gain 300 and exposure time of 1 s (Figure 1 – Figure Supplement 1B). For each
611 measurement, the field of view was chosen to contain both a small region of high density with
612 confluent cells and a few hundred well-separated single cells (Figure 1 – Figure Supplement 1C).
613 During our approximately 30 min long measurements, the focus was maintained using the Nikon
614 perfect focus system.

615

616 **Image processing and data analysis**

617 The image analysis was performed using the NIS-Elements AR software. The CFP and YFP
618 images, each recorded by a half of the camera chip (256 x 512 px², 1 px = 0.40 μ m), were
619 aligned with each other by manual image registration. A gray average of the two channels was
620 then delineated to enhance contrast and create binary masks with a user-defined, experiment-
621 specific threshold. Individual cells were detected by segmentation of the thresholded image into
622 individual objects, filtered according to size (3-50 μ m²) and shape (excentricity < 0.86). This
623 step resulted in a collection of distinct regions of interest (ROIs) for each frame of the movie.

624 The ROIs were then tracked from frame to frame, using the NIS build-in tracking algorithm.
625 Only ROIs that could be tracked over the entire duration of the experiment were further
626 analyzed. The selected ROIs were then inspected manually and those not representing individual
627 single cells well attached to the cover glass were discarded. Each individual measurement
628 contained on the order of 100 tracked single cells.

629 All further analyses were carried out using MATLAB 8.4 R2014b (The MathWorks, Inc.,
630 Natick, Massachusetts, United States). For each tracked cell, the average CFP and YFP values
631 over the ROI were extracted as a function of time. These values were also extracted for an ROI
632 corresponding to the confluent population of cells. The ratio R of the YFP signal to the CFP
633 signal was computed for both the single cells and the population, with the population response
634 being used as a reference. Cells with a FRET ratio change of less than 10% of the population
635 response were discarded as unresponsive. The PSD was computed over $T=400$ -frames long
636 segments as

$$637 \quad S_R(\omega) = \frac{1}{T} \left\langle \frac{\widehat{R}_i(\omega)\widehat{R}_i^*(\omega)}{\overline{R}_i^2} \right\rangle_i, \quad (5)$$

638 where $\widehat{R}_i(\omega)$ is the discrete Fourier transform of the FRET ratio of cell i at frequency $\omega/2\pi$, \widehat{R}_i^*
639 its complex conjugate, $\overline{\cdot}$ represents a temporal average over the given time interval and $\langle \cdot \rangle_i$ an
640 average over all single cells considered. The error for the PSD was evaluated as

$$641 \quad \frac{1}{N_c T} \text{var} \left(\frac{\widehat{R}_i(\omega)\widehat{R}_i^*(\omega)}{\overline{R}_i^2} \right)_i, \text{ where } N_c \text{ is the number of cells. The time autocorrelation function is}$$

642 simply the inverse Fourier transform of the PSD. The time autocorrelation functions were fitted
643 by $C(t) = C_0 \exp(-t/\tau_0)$, for $t > 0$ to measure the correlation time τ_0 , C_0 being a free
644 parameter accounting for the camera white shot noise. Although this fit was moderately accurate
645 ($0.96 \leq R^2 \leq 0.98$ in all cases), it provided a simple estimate of the fluctuation time scale.

646

647 **Quantification of measurement noise**

648 Contributions of technical fluctuations (vibrations, focus drift, *etc.*) and of the camera shot noise
649 to the noise on the FRET ratio was quantified using fluorescent beads (BD FACSDivaTM CS&T
650 Research beads #655050) that emit both in CFP and in YFP channels. The resulting shot noise
651 was found to be perfectly white (Figure 1 – Figure Supplement 3A). Additional negative control
652 experiments were performed using a receptorless strain, where no CheA-based signaling occurs.
653 In this case, the noise in FRET ratio was also mostly white, except at very low frequency (Figure
654 1 – Figure Supplement 3B). Where indicated, the power spectra of other strains were corrected
655 by subtracting the power spectrum of the receptorless strain, to obtain the ‘pure’ activity
656 fluctuation spectra.

657

658 **Evaluation of the conversion factor λ**

659 The value of λ , 0.10 ± 0.01 , converting FRET ratio changes to kinase activity changes, was
660 estimated using data for the $\Delta cheR \Delta cheB$ Tar^{QEQE} strain as $\lambda = \langle \bar{R}(0) \rangle - \langle \bar{R}(100 \mu M) \rangle$, the
661 difference, averaged over all cells, between the FRET ratio in buffer, where the activity should
662 be maximal (i.e., equal to one), and the ratio upon saturating stimulation with 100 μM MeAsp. A
663 similar value $\lambda = 0.09 \pm 0.01$ could be estimated in the adaptation-proficient strains, as the
664 difference between the minimal FRET ratio value reached just after stimulation with 100 μM
665 MeAsp and the maximal value reached upon removal of this stimulus. However, this latter value
666 was slightly less precise because it is not certain that full receptor activity is reached upon
667 stimulation removal, and the more reliable $\Delta cheR \Delta cheB$ value was used in all cases.

668

669 Activity sorting

670 For Tar^{QEQE} receptors in non-adapting strains, we assumed that all the receptors are fully active
671 in buffer conditions and fully inactive upon stimulation with 100 μ M MeAsp. The pathway
672 activity in each cell was thus evaluated as $A = 1 - \frac{\bar{R}(preStim-30\mu M) - \bar{R}(30\mu M)}{\bar{R}(preStim-100\mu M) - \bar{R}(100\mu M)}$. The use of the
673 two different prestimulus values in buffer enables to minimize the effect of FRET baseline
674 variation due to bleaching of fluorophores during image acquisition. Cells were then sorted
675 according to their activity and divided into n equally populated subpopulations, and for each
676 subpopulation the average PSD $\langle s_R(\omega) \rangle_A$ at average activity A of the subpopulation was
677 evaluated for the set of frequencies displayed in Figure 4 – Figure Supplement 2. This procedure
678 was implemented for several values of n , namely $n = 10, 9, 6, 5$ and 4 , and the whole resulting
679 data was used to plot $\langle s_R(\omega) \rangle_A$ as a function of A (Figure 4 – Figure Supplement 2A).

680

681 Acknowledgements

682 The authors would like to thank R. Somavanshi for assistance with experiments and N.S.
683 Wingreen and S.M. Murray for comments on the manuscript.

684

685 Competing Interests

686 The authors declare no competing interests.

687

688 References

689 [1] ten Wolde P. R., Becker N. B., Ouldrige T. E. and Mugler A. *Fundamental Limits to*
690 *Cellular Sensing*. Journal of Statistical Physics (2016) **162**, 1395, doi:10.1007/s10955-
691 015-1440-5

- 692 [2] Rao C. V., Wolf D. M. and Arkin A. P. *Control, exploitation and tolerance of*
693 *intracellular noise*. Nature (2002) **420**, 231, doi:10.1038/nature01258
- 694 [3] Tsimring L. S. *Noise in biology*. Reports on Progress in Physics (2014) **77**,
695 doi:10.1088/0034-4885/77/2/026601
- 696 [4] Raj A. and van Oudenaarden A. *Nature, Nurture, or Chance: Stochastic Gene*
697 *Expression and Its Consequences*. Cell (2008) **135**, 216, doi:10.1016/j.cell.2008.09.050
- 698 [5] Elowitz M. B., Levine A. J., Siggia E. D. and Swain P. S. *Stochastic gene expression in*
699 *a single cell*. Science (2002) **297**, 1183, doi:10.1126/science.1070919
- 700 [6] Paulsson J. *Summing up the noise in gene networks*. Nature (2004) **427**, 415,
701 doi:10.1038/nature02257
- 702 [7] Balazsi G., van Oudenaarden A. and Collins J. J. *Cellular Decision Making and*
703 *Biological Noise: From Microbes to Mammals*. Cell (2011) **144**, 910,
704 doi:10.1016/j.cell.2011.01.030
- 705 [8] Eldar A. and Elowitz M. B. *Functional roles for noise in genetic circuits*. Nature (2010)
706 **467**, 167, doi:10.1038/nature09326
- 707 [9] Korobkova E., Emonet T., Vilar J. M. G., Shimizu T. S. and Cluzel P. *From molecular*
708 *noise to behavioural variability in a single bacterium*. Nature (2004) **428**, 574,
709 doi:10.1038/nature02404
- 710 [10] Emonet T. and Cluzel P. *Relationship between cellular response and behavioral*
711 *variability in bacterial chemotaxis*. Proceedings of the National Academy of Sciences of
712 the United States of America (2008) **105**, 3304, doi:10.1073/pnas.0705463105
- 713 [11] Berg H. C. and Brown D. A. *Chemotaxis in Escherichia-Coli Analyzed by 3-*
714 *Dimensional Tracking*. Nature (1972) **239**, 500, doi:10.1038/239500a0
- 715 [12] Dufour Y. S., Gillet S., Frankel N. W., Weibel D. B. and Emonet T. *Direct Correlation*
716 *between Motile Behavior and Protein Abundance in Single Cells*. Plos Computational
717 Biology (2016) **12**, e1005041, doi:10.1371/journal.pcbi.1005041
- 718 [13] Spudich J. L. and Koshland D. E., Jr. *Non-genetic individuality: chance in the single*
719 *cell*. Nature (1976) **262**, 467, doi:10.1038/262467a0
- 720 [14] Park H., Pontius W., Guet C. C., Marko J. F., Emonet T. and Cluzel P. *Interdependence*
721 *of behavioural variability and response to small stimuli in bacteria*. Nature (2010) **468**,
722 819, doi:10.1038/nature09551

- 723 [15] He R., Zhang R. J. and Yuan J. H. *Noise-Induced Increase of Sensitivity in Bacterial*
724 *Chemotaxis*. Biophysical Journal (2016) **111**, 430, doi:10.1016/j.bpj.2016.06.013
- 725 [16] Parkinson J. S., Hazelbauer G. L. and Falke J. J. *Signaling and sensory adaptation in*
726 *Escherichia coli chemoreceptors: 2015 update*. Trends in Microbiology (2015) **23**, 257,
727 doi:10.1016/j.tim.2015.03.003
- 728 [17] Colin R. S., Victor. *Emergent properties of bacterial chemotaxis pathway*. Current
729 Opinion in Microbiology (2017) **39**, 24, doi:10.1016/j.mib.2017.07.004
- 730 [18] Shimizu T. S., Tu Y. and Berg H. C. *A modular gradient-sensing network for chemotaxis*
731 *in Escherichia coli revealed by responses to time-varying stimuli*. Mol Syst Biol (2010)
732 **6**, 382, doi:10.1038/msb.2010.37
- 733 [19] Sourjik V. and Berg H. C. *Binding of the Escherichia coli response regulator CheY to its*
734 *target measured in vivo by fluorescence resonance energy transfer*. Proceedings of the
735 National Academy of Sciences of the United States of America (2002) **99**, 12669,
736 doi:10.1073/pnas.192463199
- 737 [20] Barkai N. and Leibler S. *Robustness in simple biochemical networks*. Nature (1997)
738 **387**, 913, doi:10.1038/43199
- 739 [21] Hansen C. H., Endres R. G. and Wingreen N. S. *Chemotaxis in Escherichia coli: A*
740 *Molecular Model for Robust Precise Adaptation*. PLoS Computational Biology (2008) **4**,
741 e1, doi:10.1371/journal.pcbi.0040001
- 742 [22] Tu Y., Shimizu T. S. and Berg H. C. *Modeling the chemotactic response of Escherichia*
743 *coli to time-varying stimuli*. Proceedings of the National Academy of Sciences of the
744 United States of America (2008) **105**, 14855, doi:10.1073/pnas.0807569105
- 745 [23] Dunten P. and Koshland D. E. *Tuning the Responsiveness of a Sensory Receptor Via*
746 *Covalent Modification*. Journal of Biological Chemistry (1991) **266**, 1491,
- 747 [24] Sourjik V. and Berg H. C. *Functional interactions between receptors in bacterial*
748 *chemotaxis*. Nature (2004) **428**, 437, doi:10.1038/nature02406
- 749 [25] Li G. Y. and Weis R. M. *Covalent modification regulates ligand binding to receptor*
750 *complexes in the chemosensory system of Escherichia coli*. Cell (2000) **100**, 357,
751 doi:10.1016/S0092-8674(00)80671-6

- 752 [26] Endres R. G., Oleksiuk O., Hansen C. H., Meir Y., Sourjik V. and Wingreen N. S.
753 *Variable sizes of Escherichia coli chemoreceptor signaling teams*. *Molecular Systems*
754 *Biology* (2008) **4**, 211, doi:10.1038/Msb.2008.49
- 755 [27] Rice M. S. and Dahlquist F. W. *Sites of Deamidation and Methylation in Tsr, a Bacterial*
756 *Chemotaxis Sensory Transducer*. *Journal of Biological Chemistry* (1991) **266**, 9746,
- 757 [28] Kehry M. R., Bond M. W., Hunkapiller M. W. and Dahlquist F. W. *Enzymatic*
758 *Deamidation of Methyl-Accepting Chemotaxis Proteins in Escherichia-Coli Catalyzed by*
759 *the Cheb Gene-Product*. *Proceedings of the National Academy of Sciences of the United*
760 *States of America* (1983) **80**, 3599, doi:10.1073/pnas.80.12.3599
- 761 [29] Li M. S. and Hazelbauer G. L. *Cellular stoichiometry of the components of the*
762 *chemotaxis signaling complex*. *Journal of Bacteriology* (2004) **186**, 3687,
763 doi:10.1128/Jb.186.12.3687-3694.2004
- 764 [30] Li M. S. and Hazelbauer G. L. *Adaptational assistance in clusters of bacterial*
765 *chemoreceptors*. *Molecular Microbiology* (2005) **56**, 1617, doi:10.1111/j.1365-
766 2958.2005.04641.x
- 767 [31] Schulmeister S., Ruttorf M., Thiem S., Kentner D., Lebiez D. and Sourjik V. *Protein*
768 *exchange dynamics at chemoreceptor clusters in Escherichia coli*. *Proceedings of the*
769 *National Academy of Sciences of the United States of America* (2008) **105**, 6403,
770 doi:10.1073/pnas.071061110
- 771 [32] Tu Y. and Grinstein G. *How white noise generates power-law switching in bacterial*
772 *flagellar motors*. *Physical review letters* (2005) **94**, 208101,
773 doi:10.1103/PhysRevLett.94.208101
- 774 [33] Pontius W., Sneddon M. W. and Emonet T. *Adaptation Dynamics in Densely Clustered*
775 *Chemoreceptors*. *Plos Computational Biology* (2013) **9**, e1003230,
776 doi:10.1371/journal.pcbi.1003230
- 777 [34] Cluzel P., Surette M. and Leibler S. *An ultrasensitive bacterial motor revealed by*
778 *monitoring signaling proteins in single cells*. *Science* (2000) **287**, 1652,
779 doi:10.1126/science.287.5458.1652
- 780 [35] Taute K. M., Gude S., Tans S. J. and Shimizu T. S. *High-throughput 3D tracking of*
781 *bacteria on a standard phase contrast microscope*. *Nature Communication* (2015) **6**,
782 8776, doi:10.1038/ncomms9776

- 783 [36] Viswanathan G. M., Buldyrev S. V., Havlin S., da Luz M. G. E., Raposo E. P. and
784 Stanley H. E. *Optimizing the success of random searches*. Nature (1999) **401**, 911,
785 doi:10.1038/44831
- 786 [37] Matthaus F., Jagodic M. and Dobnikar J. *E. coli Superdiffusion and Chemotaxis-Search*
787 *Strategy, Precision, and Motility*. Biophysical Journal (2009) **97**, 946,
788 doi:10.1016/j.bpj.2009.04.065
- 789 [38] Benichou O., Loverdo C., Moreau M. and Voituriez R. *Intermittent search strategies*.
790 Reviews of Modern Physics (2011) **83**, doi:10.1103/RevModPhys.83.81
- 791 [39] Matthaus F., Mommer M. S., Curk T. and Dobnikar J. *On the Origin and Characteristics*
792 *of Noise-Induced Levy Walks of E. Coli*. Plos One (2011) **6**, e18623,
793 doi:10.1371/journal.pone.0018623
- 794 [40] Flores M., Shimizu T. S., ten Wolde P. R. and Tostevin F. *Signaling Noise Enhances*
795 *Chemotactic Drift of E. coli*. Physical Review Letters (2012) **109**, 148101,
796 doi:10.1103/PhysRevLett.109.148101
- 797 [41] Gegner J. A., Graham D. R., Roth A. F. and Dahlquist F. W. *Assembly of an Mcp*
798 *Receptor, Chew, and Kinase Chea Complex in the Bacterial Chemotaxis Signal*
799 *Transduction Pathway*. Cell (1992) **70**, 975, doi:10.1016/0092-8674(92)90247-A
- 800 [42] Frank V. and Vaknin A. *Prolonged stimuli alter the bacterial chemosensory clusters*.
801 Molecular Microbiology (2013) **88**, 634, doi:10.1111/mmi.12215
- 802 [43] Tu Y. *Quantitative modeling of bacterial chemotaxis: signal amplification and accurate*
803 *adaptation*. Annual Review of Biophysics (2013) **42**, 337, doi:10.1146/annurev-biophys-
804 083012-130358
- 805 [44] Pinas G. E., Frank V., Vaknin A. and Parkinson J. S. *The source of high signal*
806 *cooperativity in bacterial chemosensory arrays*. Proceedings of the National Academy of
807 Sciences of the United States of America (2016) **113**, 3335,
808 doi:10.1073/pnas.1600216113
- 809 [45] Duke T. A. J. and Bray D. *Heightened sensitivity of a lattice of membrane receptors*.
810 Proceedings of the National Academy of Sciences of the United States of America (1999)
811 **96**, 10104, doi:10.1073/pnas.96.18.10104
- 812 [46] Mello B. A. and Tu Y. *Quantitative modeling of sensitivity in bacterial chemotaxis: the*
813 *role of coupling among different chemoreceptor species*. Proceedings of the National

- 814 Academy of Sciences of the United States of America (2003) **100**, 8223,
815 doi:10.1073/pnas.1330839100
- 816 [47] Monod J., Wyman J. and Changeux J. P. *On Nature of Allosteric Transitions - a*
817 *Plausible Model*. Journal of Molecular Biology (1965) **12**, 88, doi:10.1016/S0022-
818 2836(65)80285-6
- 819 [48] Keymer J. E., Endres R. G., Skoge M., Meir Y. and Wingreen N. S. *Chemosensing in*
820 *Escherichia coli: Two regimes of two-state receptors*. Proceedings of the National
821 Academy of Sciences of the United States of America (2006) **103**, 1786,
822 doi:10.1073/pnas.0507438103
- 823 [49] Mello B. A. and Tu Y. *An allosteric model for heterogeneous receptor complexes:*
824 *understanding bacterial chemotaxis responses to multiple stimuli*. Proc Natl Acad Sci U
825 S A (2005) **102**, 17354, doi:10.1073/pnas.0506961102
- 826 [50] Sourjik V., Vaknin A., Shimizu T. S. and Berg H. C. *In vivo measurement by FRET of*
827 *pathway activity in bacterial chemotaxis*. Methods Enzymology (2007) **423**, 365,
828 doi:10.1016/S0076-6879(07)23017-4
- 829 [51] Sourjik V. and Berg H. C. *Receptor sensitivity in bacterial chemotaxis*. Proceedings of
830 the National Academy of Sciences of the United States of America (2002) **99**, 123,
831 doi:10.1073/pnas.011589998
- 832 [52] Oleksiuk O., Jakovljevic V., Vladimirov N., Carvalho R., Paster E., Ryu W. S., Meir Y.,
833 Wingreen N. S., Kollmann M. and Sourjik V. *Thermal robustness of signaling in*
834 *bacterial chemotaxis*. Cell (2011) **145**, 312, doi:10.1016/j.cell.2011.03.013
- 835 [53] Neumann S., Vladimirov N., Krembel A. K., Wingreen N. S. and Sourjik V. *Imprecision*
836 *of Adaptation in Escherichia coli Chemotaxis*. PLoS ONE (2014) **9**, e84904,
837 doi:10.1371/journal.pone.0084904
- 838 [54] Krembel A. K., Neumann S. and Sourjik V. *Universal response-adaptation relation in*
839 *bacterial chemotaxis*. Journal of Bacteriology (2014) JB.02171, doi:10.1128/JB.02171-
840 14
- 841 [55] Meir Y., Jakovljevic V., Oleksiuk O., Sourjik V. and Wingreen N. S. *Precision and*
842 *Kinetics of Adaptation in Bacterial Chemotaxis*. Biophysical Journal (2010) **99**, 2766,
843 doi:10.1016/j.bpj.2010.08.051

- 844 [56] Frank V., Pinas G. E., Cohen H., Parkinson J. S. and Vaknin A. *Networked*
845 *Chemoreceptors Benefit Bacterial Chemotaxis Performance*. MBio (2016) **7**, e01824,
846 doi:10.1128/mBio.01824-16
- 847 [57] Krembel A., Colin R. and Sourjik V. *Importance of Multiple Methylation Sites in*
848 *Escherichia coli Chemotaxis*. PLoS One (2015) **10**, e0145582,
849 doi:10.1371/journal.pone.0145582
- 850 [58] Neumann S., Lovdok L., Bentele K., Meisig J., Ullner E., Paldy F. S., Sourjik V. and
851 Kollmann M. *Exponential Signaling Gain at the Receptor Level Enhances Signal-to-*
852 *Noise Ratio in Bacterial Chemotaxis*. Plos One (2014) **9**, e0087815,
853 doi:10.1371/journal.pone.0087815
- 854 [59] Neumann S., Grosse K. and Sourjik V. *Chemotactic signaling via carbohydrate*
855 *phosphotransferase systems in Escherichia coli*. Proceedings of the National Academy
856 of Sciences of the United States of America (2012) **109**, 12159,
857 doi:10.1073/pnas.1205307109
- 858 [60] Clausznitzer D., Oleksiuk O., Løvdok L., Sourjik V. and Endres R. G. *Chemotactic*
859 *Response and Adaptation Dynamics in Escherichia coli*. PLoS Computational Biology
860 (2010) **6**, e1000784, doi:10.1371/journal.pcbi.1000784
- 861 [61] Berg H. C. and Tedesco P. M. *Transient-Response to Chemotactic Stimuli in*
862 *Escherichia-Coli*. Proceedings of the National Academy of Sciences of the United States
863 of America (1975) **72**, 3235, doi:10.1073/pnas.72.8.3235
- 864 [62] Gasquet C. and Witomski P. *Fourier analysis and applications: filtering, numerical*
865 *computation, wavelets, volume 30 of Texts in applied mathematics*. (1999) Springer-
866 Verlag, Berlin, Germany
- 867 [63] Li M. and Hazelbauer G. L. *Selective allosteric coupling in core chemotaxis signaling*
868 *complexes*. Proceedings of the National Academy of Sciences of the United States of
869 America (2014) **111**, 15940, doi:10.1073/pnas.1415184111
- 870 [64] Kubo R. *Fluctuation-Dissipation Theorem*. Reports on Progress in Physics (1966) **29**,
871 255, doi:10.1088/0034-4885/29/1/306
- 872 [65] Robert D., Nguyen T. H., Gallet F. and Wilhelm C. *In Vivo Determination of Fluctuating*
873 *Forces during Endosome Trafficking Using a Combination of Active and Passive*
874 *Microrheology*. Plos One (2010) **5**, e10046, doi:10.1371/journal.pone.0010046

- 875 [66] Martin P., Hudspeth A. J. and Julicher F. *Comparison of a hair bundle's spontaneous*
876 *oscillations with its response to mechanical stimulation reveals the underlying active*
877 *process*. Proceedings of the National Academy of Sciences of the United States of
878 America (2001) **98**, 14380, doi:10.1073/pnas.251530598
- 879 [67] Mizuno D., Tardin C., Schmidt C. F. and MacKintosh F. C. *Nonequilibrium mechanics*
880 *of active cytoskeletal networks*. Science (2007) **315**, 370, doi:10.1126/science.1134404
- 881 [68] Cugliandolo L. F. *The effective temperature*. Journal of Physics a-Mathematical and
882 Theoretical (2011) **44**, doi:10.1088/1751-8113/44/48/483001
- 883 [69] Hansen C. H., Sourjik V. and Wingreen N. S. *A dynamic-signaling-team model for*
884 *chemotaxis receptors in Escherichia coli*. Proceedings of the National Academy of
885 Sciences of the United States of America (2010) **107**, 17170,
886 doi:10.1073/pnas.1005017107
- 887 [70] Shimizu T. S., Aksenov S. V. and Bray D. *A spatially extended stochastic model of the*
888 *bacterial chemotaxis signalling pathway*. Journal of Molecular Biology (2003) **329**, 291,
889 doi:10.1016/S0022-2836(03)00437-6
- 890 [71] Wang P., Song C. M. and Makse H. A. *Dynamic particle tracking reveals the ageing*
891 *temperature of a colloidal glass*. Nature Physics (2006) **2**, 526, doi:10.1038/nphys366
- 892 [72] Abou B. and Gallet F. *Probing a nonequilibrium Einstein relation in an aging colloidal*
893 *glass*. Physical Review Letters (2004) **93**, 160603, doi:10.1103/PhysRevLett.93.160603
- 894 [73] Mello B. A. and Tu Y. *Effects of adaptation in maintaining high sensitivity over a wide*
895 *range of backgrounds for Escherichia coli chemotaxis*. Biophysical journal (2007) **92**,
896 2329, doi:10.1529/biophysj.106.097808
- 897 [74] Sartori P. and Tu Y. H. *Free Energy Cost of Reducing Noise while Maintaining a High*
898 *Sensitivity*. Physical Review Letters (2015) **115**, 118102,
899 doi:10.1103/PhysRevLett.115.118102
- 900 [75] Clausznitzer D. and Endres R. G. *Noise characteristics of the Escherichia coli rotary*
901 *motor*. BMC Systems Biology (2011) **5**, 151, doi:10.1186/1752-0509-5-151
- 902 [76] Sartori P. and Tu Y. *Noise filtering strategies in adaptive biochemical signaling*
903 *networks: Application to E. coli chemotaxis*. Journal of statistical physics (2011) **142**,
904 1206, doi:10.1007/s10955-011-0169-z

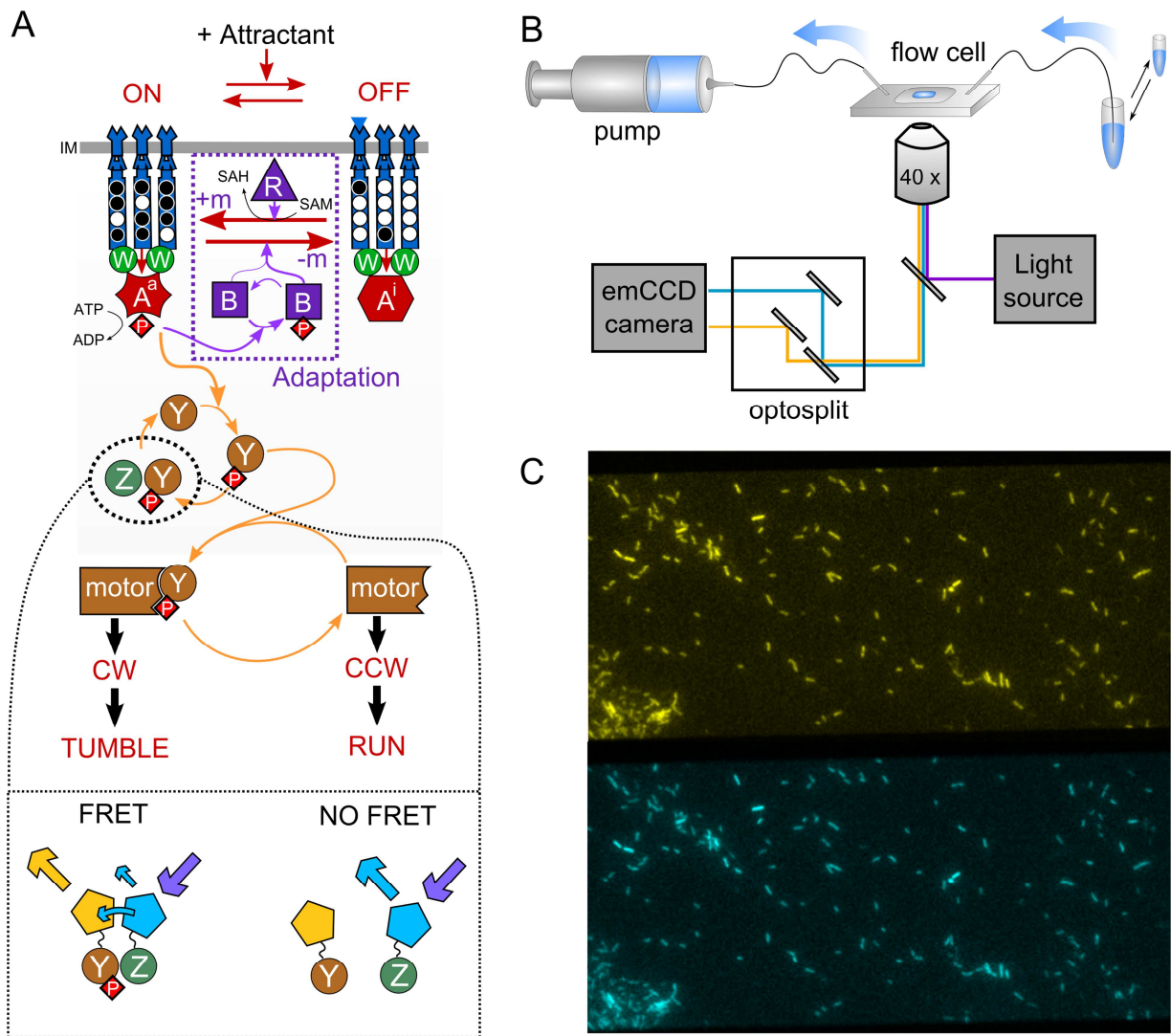
- 905 [77] Aquino G., Clausznitzer D., Tollis S. and Endres R. G. *Optimal receptor-cluster size*
906 *determined by intrinsic and extrinsic noise*. Physical Review E (2011) **83**, 021914,
907 doi:10.1103/Physreve.83.021914
- 908 [78] Conlon P., Gelin-Licht R., Ganesan A., Zhang J. and Levchenko A. *Single-cell dynamics*
909 *and variability of MAPK activity in a yeast differentiation pathway*. Proceedings of the
910 National Academy of Sciences of the United States of America (2016) **113**, E5896,
911 doi:10.1073/pnas.1610081113
- 912 [79] Aoki K., Kumagai Y., Sakurai A., Komatsu N., Fujita Y., Shionyu C. and Matsuda M.
913 *Stochastic ERK Activation Induced by Noise and Cell-to-Cell Propagation Regulates Cell*
914 *Density-Dependent Proliferation*. Molecular Cell (2013) **52**, 529,
915 doi:10.1016/j.molcel.2013.09.015
- 916 [80] Paliwal S., Iglesias P. A., Campbell K., Hilioti Z., Groisman A. and Levchenko A.
917 *MAPK-mediated bimodal gene expression and adaptive gradient sensing in yeast*.
918 Nature (2007) **446**, 46, doi:10.1038/nature05561
- 919 [81] Bowsher C. G. and Swain P. S. *Identifying sources of variation and the flow of*
920 *information in biochemical networks*. Proceedings of the National Academy of Sciences
921 of the United States of America (2012) **109**, E1320, doi:10.1073/pnas.1119407109
- 922 [82] Sourjik V. and Wingreen N. S. *Responding to chemical gradients: bacterial chemotaxis*.
923 Current Opinion in Cell Biology (2012) **24**, 262, doi:10.1016/j.ceb.2011.11.008
- 924 [83] Micali G. and Endres R. G. *Bacterial chemotaxis: information processing,*
925 *thermodynamics, and behavior*. Current Opinion in Microbiology (2016) **30**, 8,
926 doi:10.1016/j.mib.2015.12.001
- 927 [84] Yi T. M., Huang Y., Simon M. I. and Doyle J. *Robust perfect adaptation in bacterial*
928 *chemotaxis through integral feedback control*. Proceedings of the National Academy of
929 Sciences of the United States of America (2000) **97**, 4649, doi:10.1073/pnas.97.9.4649
- 930 [85] Kollmann M., Lovdok L., Bartholome K., Timmer J. and Sourjik V. *Design principles of*
931 *a bacterial signalling network*. Nature (2005) **438**, 504, doi:10.1038/nature04228
- 932 [86] Alon U., Surette M. G., Barkai N. and Leibler S. *Robustness in bacterial chemotaxis*.
933 Nature (1999) **397**, 168, doi:10.1038/16483

- 934 [87] Chevy L., Colin R., Abou B. and Berret J. F. *Intracellular micro-rheology probed by*
935 *micron-sized wires*. *Biomaterials* (2013) **34**, 6299,
936 doi:10.1016/j.biomaterials.2013.05.002
- 937 [88] Bialek W. and Setayeshgar S. *Physical limits to biochemical signaling*. *Proceedings of*
938 *the National Academy of Sciences of the United States of America* (2005) **102**, 10040,
939 doi:10.1073/pnas.0504321102
- 940 [89] Seifert U. *Stochastic thermodynamics, fluctuation theorems and molecular machines*.
941 *Reports on Progress in Physics* (2012) **75**, 126001, doi:10.1088/0034-4885/75/12/126001
- 942 [90] Lan G., Sartori P., Neumann S., Sourjik V. and Tu Y. H. *The energy-speed-accuracy*
943 *trade-off in sensory adaptation*. *Nature Physics* (2012) **8**, 422, doi:10.1038/Nphys2276
- 944 [91] Skoge M. L., Endres R. G. and Wingreen N. S. *Receptor-receptor coupling in bacterial*
945 *chemotaxis: Evidence for strongly coupled clusters*. *Biophysical Journal* (2006) **90**,
946 4317, doi:10.1529/biophysj.105.079905
- 947 [92] Kalinin Y. V., Jiang L., Tu Y. and Wu M. *Logarithmic sensing in Escherichia coli*
948 *bacterial chemotaxis*. *Biophys J* (2009) **96**, 2439, doi:10.1016/j.bpj.2008.10.027
- 949 [93] Vladimirov N., Lovdok L., Lebiez D. and Sourjik V. *Dependence of Bacterial*
950 *Chemotaxis on Gradient Shape and Adaptation Rate*. *Plos Computational Biology*
951 (2008) **4**, e1000242, doi:10.1371/journal.pcbi.1000242
- 952 [94] Berg H. C. *The rotary motor of bacterial flagella*. *Annual Review of Biochemistry*
953 (2003) **72**, 19, doi:10.1146/annurev.biochem.72.121801.161737
- 954 [95] Peng C. K., Mietus J., Hausdorff J. M., Havlin S., Stanley H. E. and Goldberger A. L.
955 *Long-range anticorrelations and non-Gaussian behavior of the heartbeat*. *Phys Rev Lett*
956 (1993) **70**, 1343, doi:10.1103/PhysRevLett.70.1343
- 957 [96] Clausznitzer D., Oleksiuk O., Lovdok L., Sourjik V. and Endres R. G. *Chemotactic*
958 *Response and Adaptation Dynamics in Escherichia coli*. *Plos Computational Biology*
959 (2010) **6**, e1000784, doi:10.1371/journal.pcbi.1000784

960

961

962 **Supplementary Figures**



963

964 **Figure 1 – Figure Supplement 1. Schematic representation of the FRET experiment. (A)**

965 The phosphorylation-dependent monitoring of the chemotaxis pathway activity via FRET. CheY

966 and CheZ are tagged with the two components of a FRET pair of fluorophores, so that the level

967 of energy transfer represents the amount of CheY-CheZ interaction. This quantity reflects then

968 the fraction of phosphorylated CheY-P, which represents the average fraction of active CheA

969 (A^a) on the second time scale, because of the rapid cycle of (de)phosphorylation of CheY by

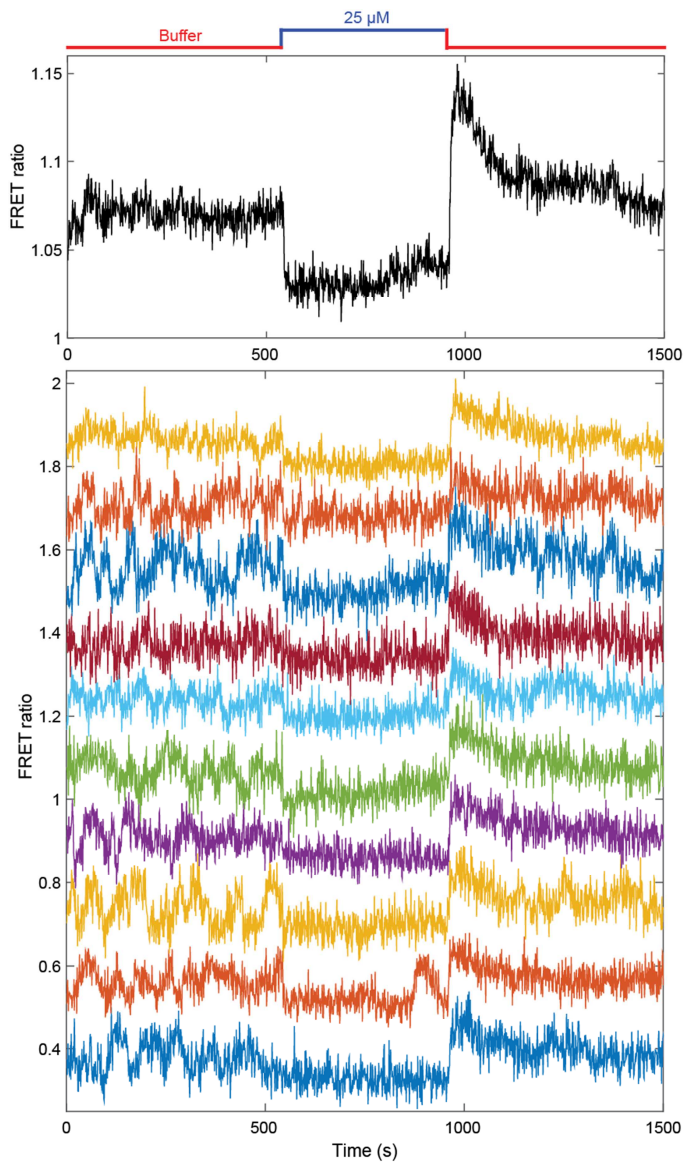
970 CheA^a and CheZ. See text for further explanations. (B) Schematic of the experimental device.

971 Media containing chemoeffectors are flown over the cells attached to a coverslip. Cell

972 fluorescence is observed simultaneously in two spectral channels separated by an optosplit and
973 an EM-CCD camera. (C) Typical recorded image, showing in the order of a hundred single cells
974 and a small group of cells, the FRET measurement of which is used as a reference during the
975 experiment.

976

977

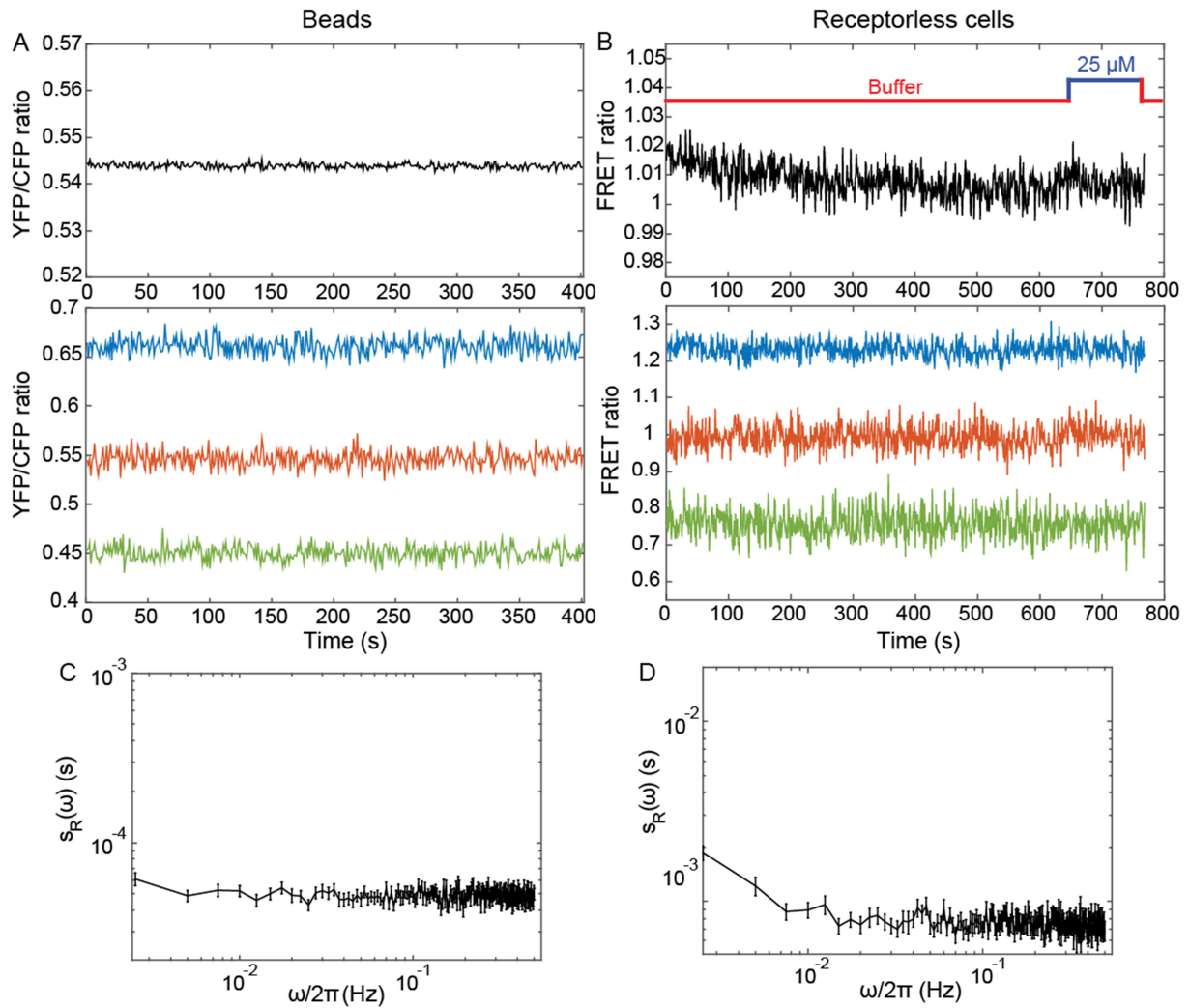


978

979 **Figure 1 – Figure Supplement 2. Additional FRET measurement for CheR⁺ CheB⁺ cells.**

980 Population averaged FRET ratio (top) and corresponding single cell FRET ratios (bottom), for a
981 typical FRET experiment, with adaptation-proficient strain expressing Tar^{QEQE} as the sole
982 receptor. Cells initially adapted in buffer were stimulated with 25 μM MeAsp, before returning
983 to buffer. FRET ratios for individual cells have been shifted to facilitate visualization.

984



985

986 **Figure 1 – Figure Supplement 3. Negative controls.** (A,B) Average (top) and individual

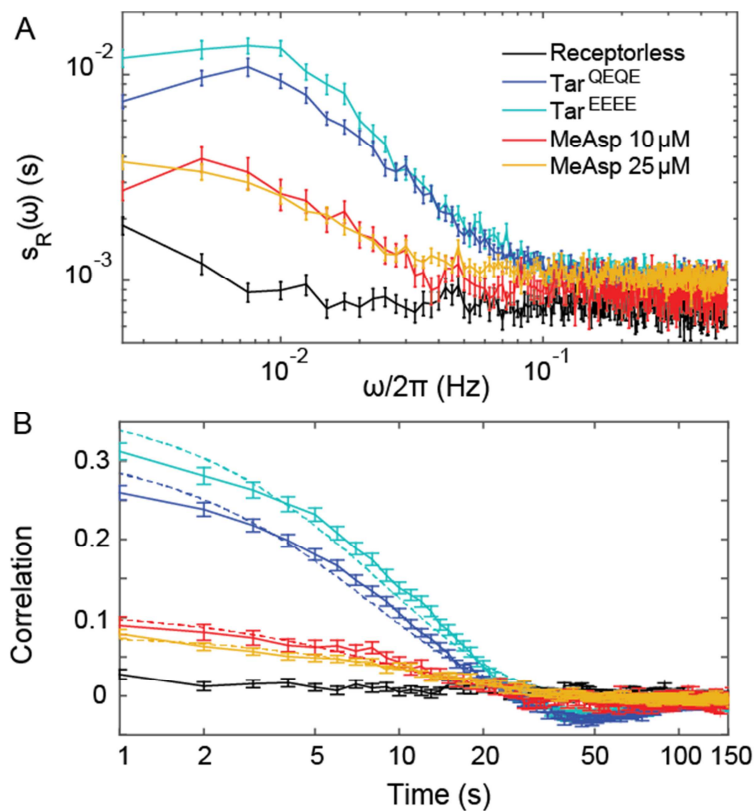
987 (bottom) measurements of the YFP/CFP ratio for fluorescent beads emitting both in CFP and

988 YFP channels (A) and for receptorless cells expressing FRET pair (B). (C,D) The corresponding

989 PSDs of the fluorescent beads and of the receptorless cells. Error bars represent standard errors

990 of the mean (SEM) and sample sizes are 189 (beads) and 103 (receptorless strain) single objects.

991



992

993 **Figure 1 – Figure Supplement 4. Additional analyses for CheR⁺ CheB⁺ cells.** Same as Figure

994 1B,C but also including the PSDs (A) and time autocorrelation functions (B) of the FRET ratio

995 measured for CheR⁺ CheB⁺ cells expressing Tar^{EEEE} and adapted in buffer or expressing Tar^{QEQE}

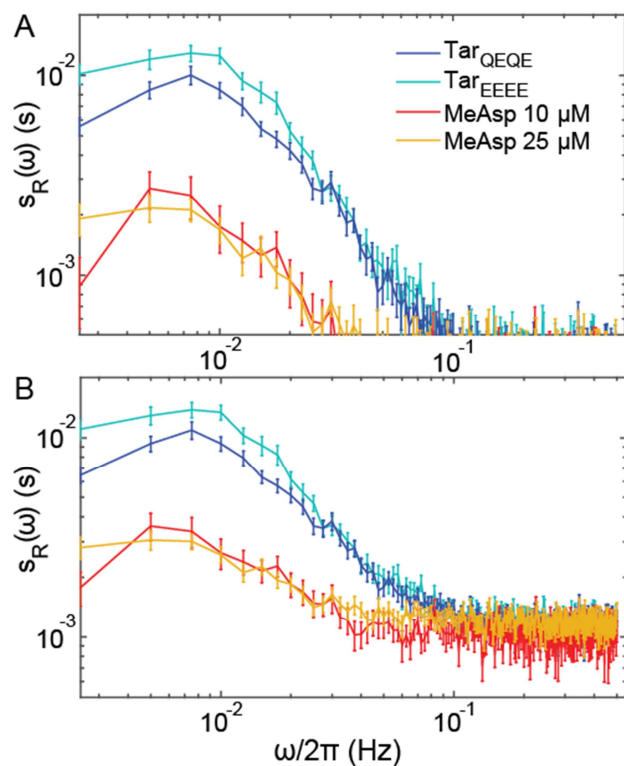
996 and adapted to 25 μ M MeAsp. The error bars represent SEM, and the sample sizes are 103

997 (receptorless strain), 203 (Tar^{EEEE} in buffer), 265 (Tar^{QEQE} in buffer), 69 (10 μ M) and 219 (25

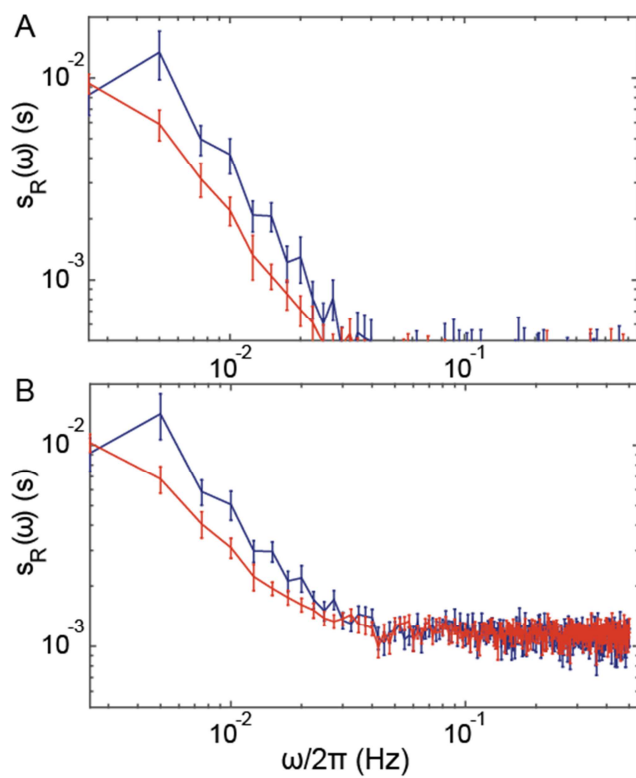
998 μ M) single cells coming from at least three independent experiments in each case.

999

1000



1001
1002 **Figure 1 – Figure Supplement 5. Correction of the PSDs for CheR⁺ CheB⁺ cells for**
1003 **measurement noise.** (A) The PSDs for the different conditions (colors as in Figure Supplement
1004 4) from which the PSD of the receptorless strain (representing measurement noise) was
1005 subtracted. (B) Same curves as (A) but with added constant value (9×10^{-4} s), in order to compare
1006 with Figure 1B. Statistics is as in Figure 1 – Figure supplement 4.
1007

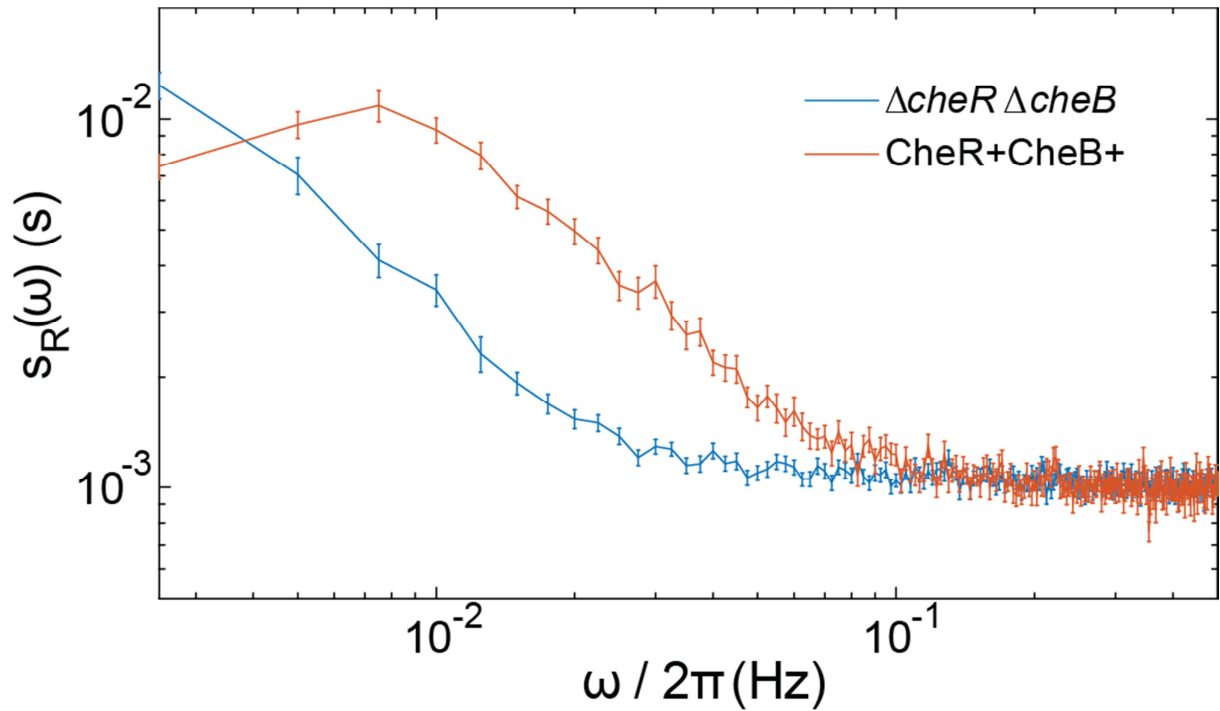


1008

1009 **Figure 2 – Figure Supplement 1. Correction of the PSDs for $\Delta cheR\Delta cheB$ cells for**
1010 **measurement noise.** Same as Figure 1 – Figure Supplement 5 but for $\Delta cheR\Delta cheB$ cells.

1011 Statistics is as in the main Figure 2.

1012



1013

1014 **Figure 2 – Figure Supplement 2. Comparison of $\Delta cheR\Delta cheB$ and $CheR^+ CheB^+$ power**

1015 **spectra.** The PSDs of the FRET ratio are plotted for the $\Delta cheR\Delta cheB$ strain expressing Tar^{QEQE}

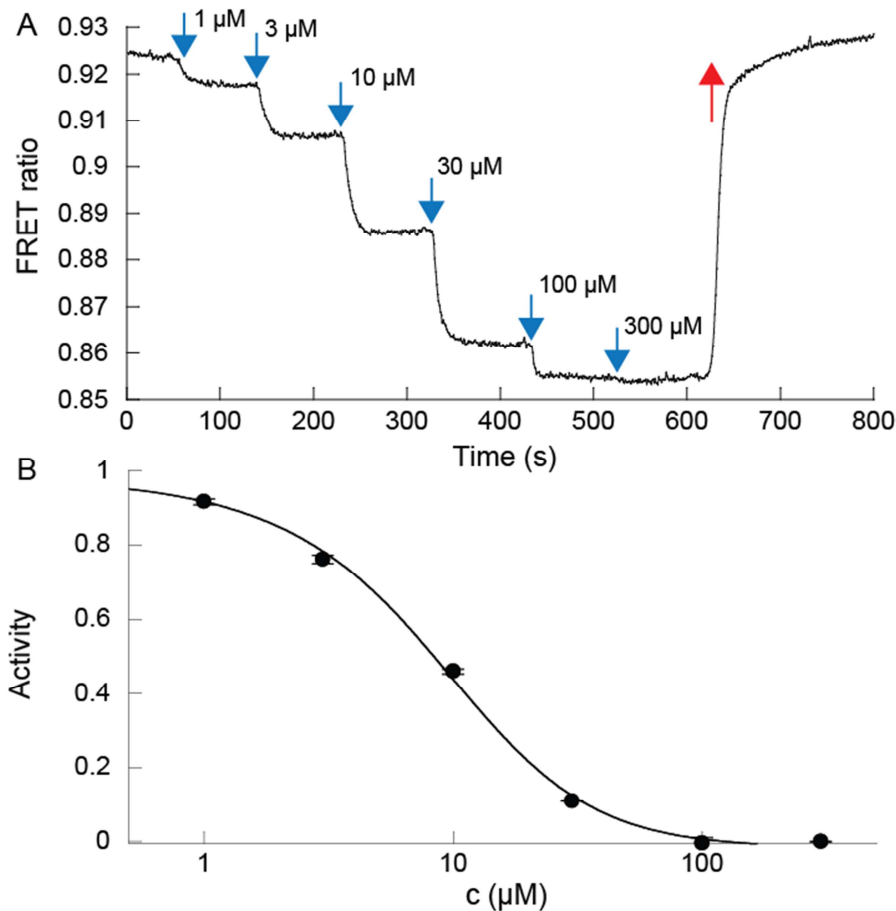
1016 as sole receptor and stimulated with 30 μM MeAsp (blue) and the $CheR^+ CheB^+$ strain

1017 expressing Tar^{QEQE} as sole receptor and adapted in buffer (red). The error bars represent

1018 standard errors of the mean (SEM), and the sample sizes are 265 ($CheR^+ CheB^+$) and 540

1019 ($\Delta cheR\Delta cheB$) single cells coming from at least three independent experiments in each case.

1020



1021

1022 **Figure 3 – Figure Supplement 1. Dose response to MeAsp of $\Delta cheR\Delta cheB$ CheW-X2 cells**

1023 **expressing Tar^{QEQE} .** (A) Example of the FRET ratio (R) decreasing as increasing amounts of

1024 MeAsp were delivered to the cells. (B) The activity averaged over two biological replicates was

1025 estimated as $(R(c) - R_{min}) / (R_{max} - R_{min})$, plotted as a function of MeAsp concentration c ,

1026 and fitted using the Monod-Wyman-Changeux model, assuming a free energy difference in

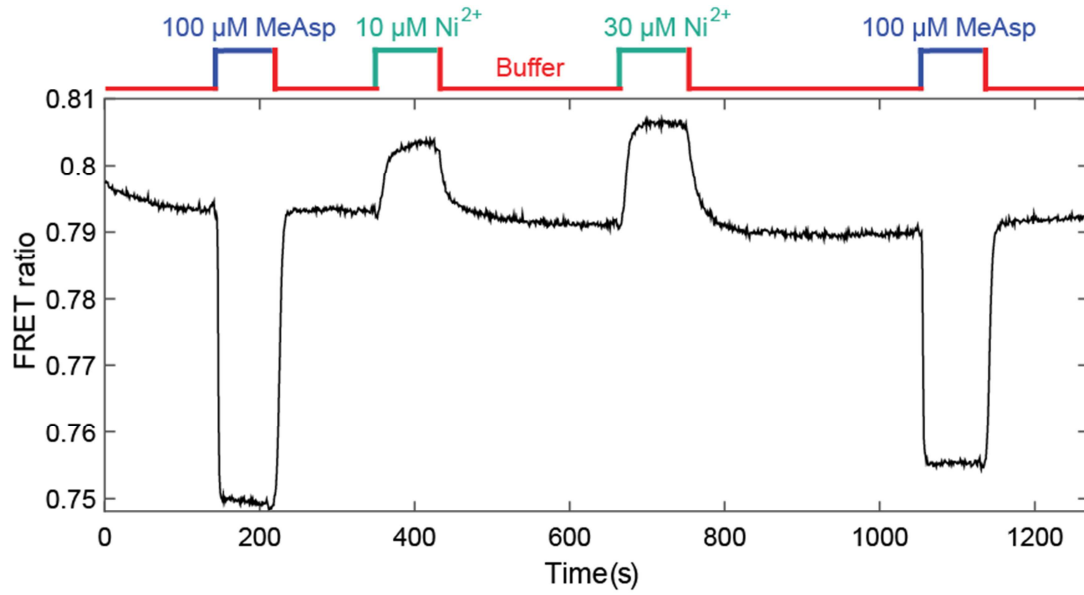
1027 absence of ligand $\gamma(m = 2) = -1$, yielding a cooperativity number $N = 1.73$ and a binding

1028 constant to inactive receptors $K_{OFF} = 3.92 \mu M$. Fitting with a Hill function yields a Hill exponent

1029 $H = 1.4$ and a concentration of half-maximal response $EC_{50} = 8.3 \mu M$. Error bars indicate SEM.

1030 Measurements were carried out on confluent populations of cells.

1031



1032

1033 **Figure 3 – Figure Supplement 2. Response of CheR⁺ CheB⁺ strain expressing CheW-X2**

1034 **and Tar^{QEQE} to attractant MeAsp and repellent Ni²⁺.** The activity dropped in response to

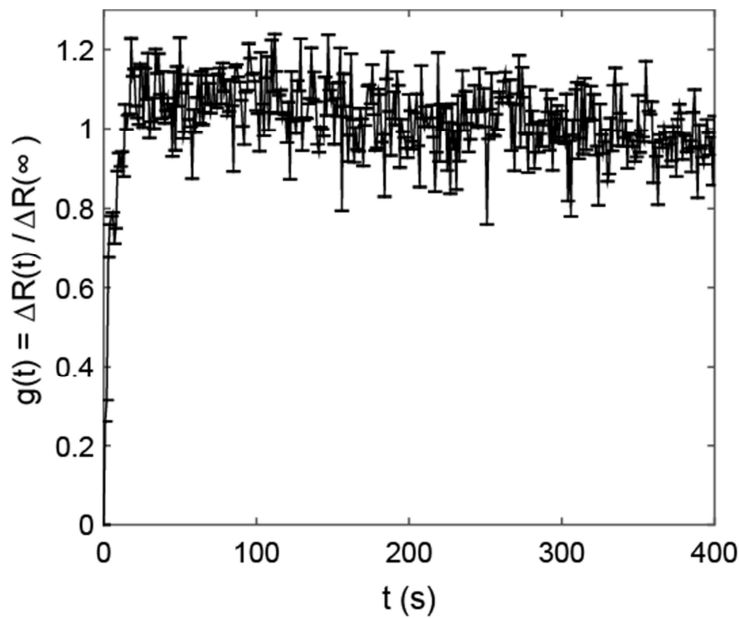
1035 MeAsp and increased in response to Ni²⁺, added at indicated concentrations, demonstrating that

1036 the cells have indeed an intermediate level of adapted kinase activity. The buffer for this

1037 experiment did not contain EDTA, an ion chelator for Ni²⁺.

1038

1039



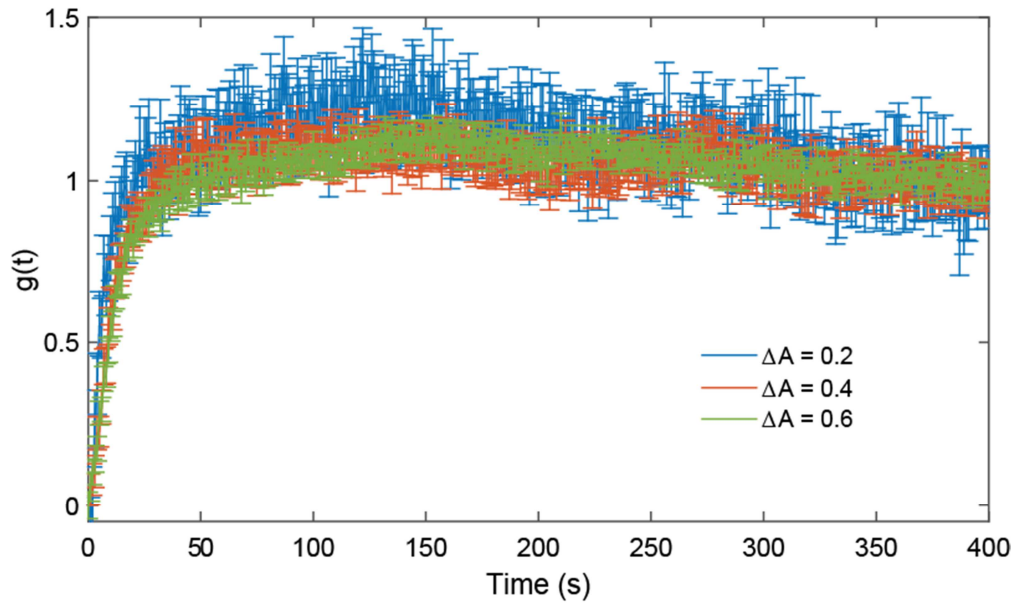
1040

1041 **Figure 3 – Figure Supplement 3. Response function for $\Delta cheR\Delta cheB$ CheW-X2 cells**

1042 **expressing Tar^{QEQE} as sole receptor.** The strain was subjected to 10 μ M MeAsp to measure the

1043 response. Error bars indicate SEM and sample size is 120 single cells, in 3 biological replicates.

1044



1045

1046 **Figure 4 – Figure Supplement 1. Validation of the linear response regime in $\Delta cheR\Delta cheB$**

1047 **cells.** Response functions measured for stimulations by increasing MeAsp concentration from 25

1048 to 30 μM , corresponding to an average activity change of 0.2 (blue), from 0 to 25 μM ,

1049 corresponding to an average activity change of 0.4 (red), and from 0 to 30 μM corresponding to

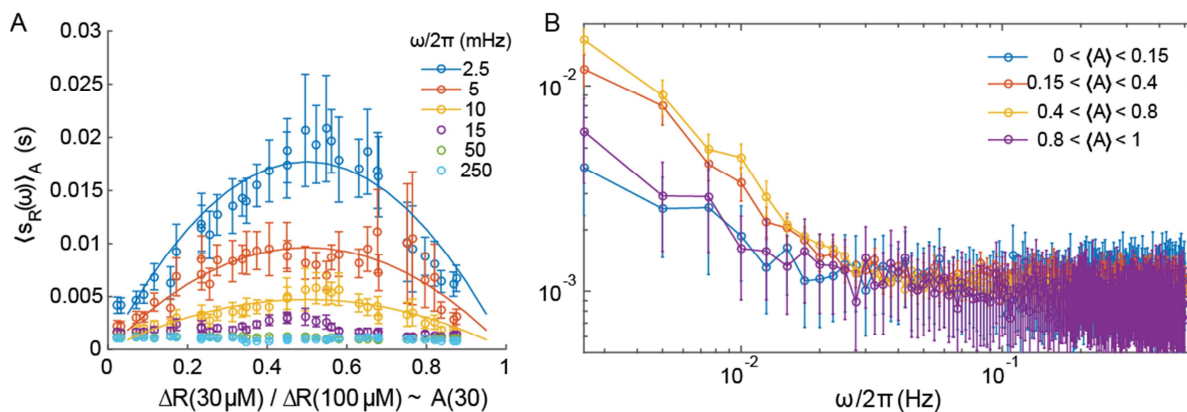
1050 an average activity change of 0.6 (green; data from the main figure). Error bars represent SEM

1051 and sample sizes are 339 ($\Delta A = 0.2$ and $\Delta A = 0.4$) and 540 ($\Delta A = 0.6$) single cells in at least

1052 three biological replicates.

1053

1054



1055

1056 **Figure 4 – Figure Supplement 2. Power spectral density computed on subsets of the cell**

1057 **populations sorted according to their activity.** (A) The PSD as a function of the average

1058 activity of the subsets, for the indicated frequencies (dots) in the $\Delta cheR\Delta cheB$ strain expressing

1059 $Tar^{QE QE}$. The lines correspond to best fits by $\langle s_R(\omega) \rangle_A = C(\omega)A(30)(1 - A(30))$ for each

1060 frequency considered. (B) The PSD as a function of frequency for subsets of cells sorted

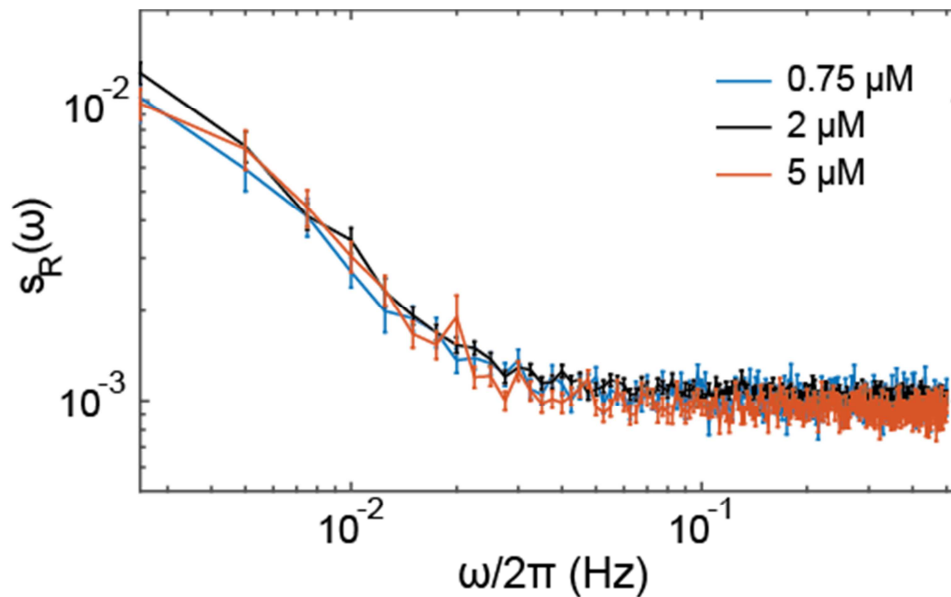
1061 according to their activity as indicated in the legend. The error bars correspond to SEM, sample

1062 sizes are as described in Materials and methods, varying from 54 to 135 cells depending on the

1063 point, taken from at least 5 biological replicates.

1064

1065



1066

1067 **Figure 4 – Figure Supplement 3. Effect of the receptor expression level on the noise in**

1068 ***$\Delta cheR\Delta cheB$* cells.** The $\Delta cheR\Delta cheB$ strain expressing Tar^{QEQE} as the sole receptor from a

1069 plasmid under salicylate induction, was induced by 0.75 μM , 2 μM (standard experimental

1070 condition used in the main text) or 5 μM salicylate, resulting in approximately two-fold

1071 difference between the protein numbers [26]. The power spectral density of fluctuation in cells

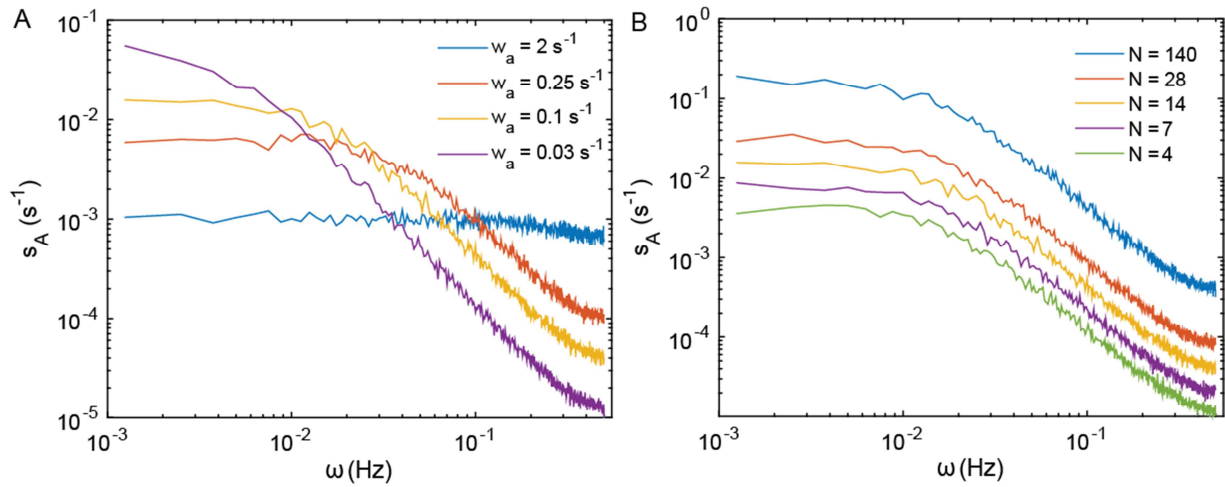
1072 prestimulated with 30 μM MeAsp, with average activity $A = 0.5$, was the same in all conditions.

1073 Error bars indicate SEM and sample sizes are 237 (5 μM), 540 (2 μM) and 187 (0.75 μM) cells in

1074 at least three biological replicates.

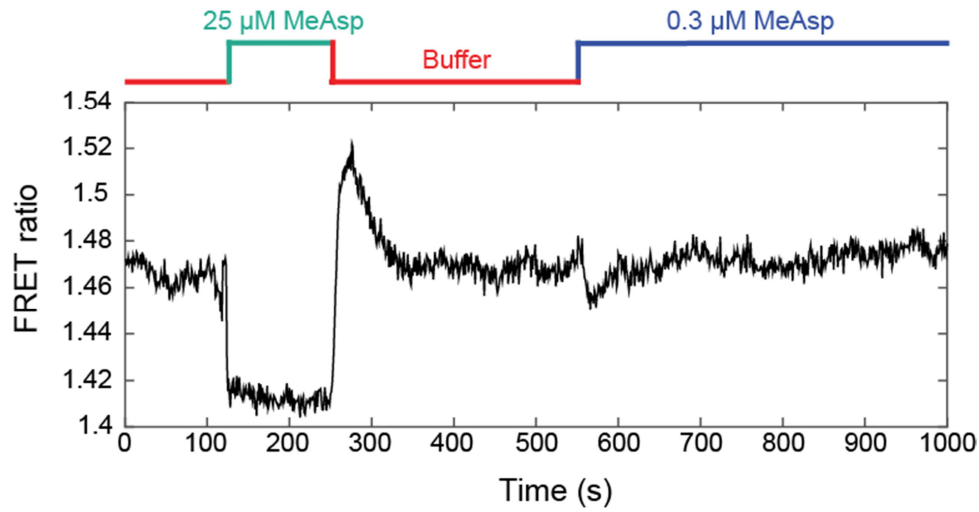
1075

1076



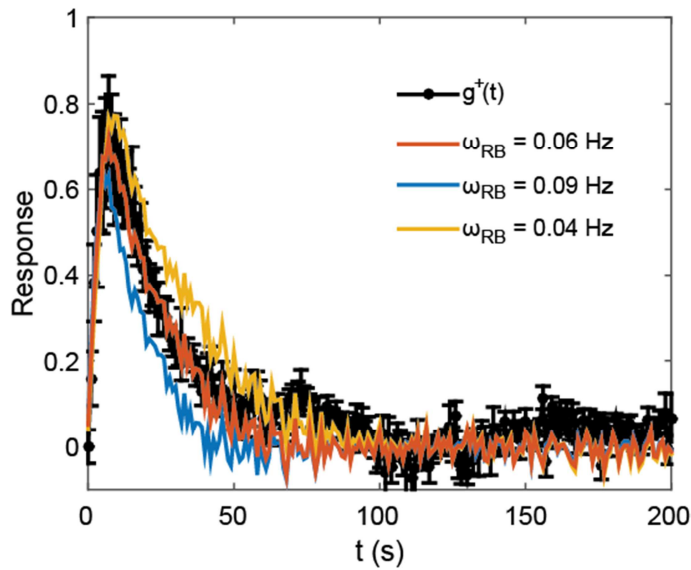
1077

1078 **Figure 4 – Figure Supplement 4. Power spectra of thermal fluctuations in a simulated**
1079 **model of the sensory cluster.** The model describes behavior of cooperative receptor complexes
1080 without adaptation (see Appendix, section 4). Dependence of the PSD of the mean activity of the
1081 receptor cluster $s_A(\omega)$ on the rate of cluster response w_a to free energy perturbations at fixed
1082 number of allosteric units per team $N = 14$ (A) and on N at fixed $w_a = 0.25 \text{ s}^{-1}$ (B). The total
1083 number of chemoreceptors was kept constant in all cases.



1085 **Figure 4 – Figure Supplement 5. Example of FRET measurement used for the evaluation of**
1086 **$g^+(t)$.** A CheR⁺ CheB⁺ strain expressing Tar^{QEQE} as sole receptor and the CheY-YFP/CheZ-CFP
1087 FRET pair, equilibrated in buffer (red), was briefly stimulated with a saturating amount of
1088 MeAsp (25 μM; green) to evaluate the FRET ratio at zero activity, re-equilibrated in buffer, and
1089 then stimulated with a subsaturating amount of MeAsp (0.3 μM; blue). The FRET ratio was
1090 measured on an area of confluent cells. Normalized responses to 0.3 μM MeAsp from five
1091 independent replicates of this experiment were averaged to compute the step response function
1092 of Figure 4A.

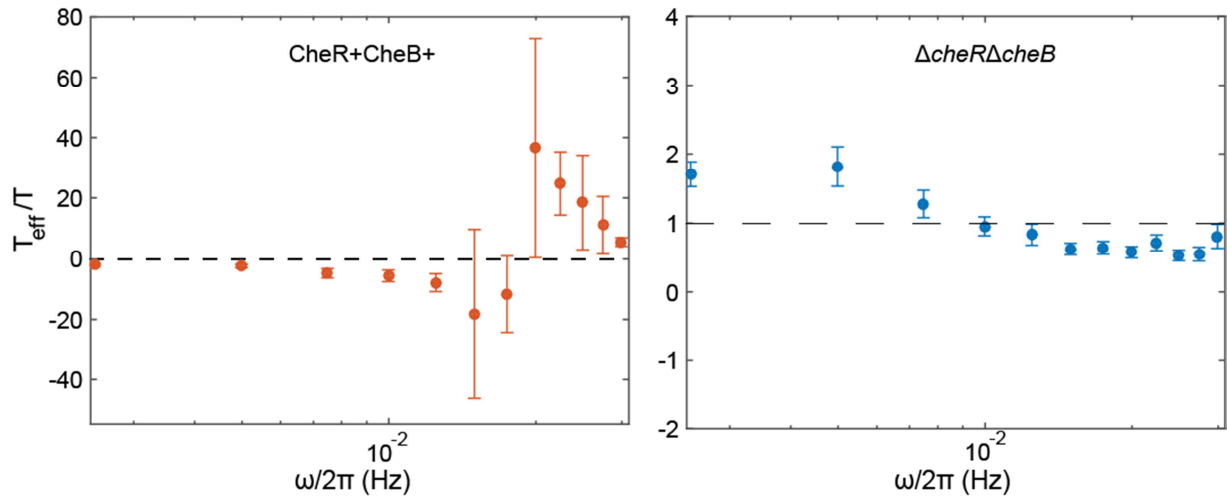
1093



1094

1095 **Figure 4 – Figure Supplement 6. Evaluation of the adaptation time.** The normalized step
1096 response function in $\text{CheR}^+ \text{CheB}^+$, $g^+(t)$, from Figure 4A is plotted alongside its fits by
1097 Equation (A.30) of the Appendix, using the normalized step response function in $\Delta\text{cheR}\Delta\text{cheB}$
1098 strain, $g^-(t)$, and the rate of adaptation at the activity level ω_{RB} , for various values of ω_{RB} . The
1099 best fit was with $\omega_{RB} = 0.06$. The response function was measured over five areas of confluent
1100 cells from as many independent experiments.

1101



1102

1103 **Figure 4 – Figure Supplement 7. Calculated effective temperatures.** Plots show the inverse of

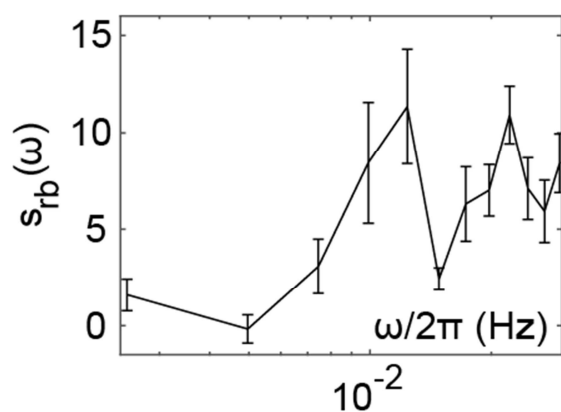
1104 the quantities plotted in insets of Figure 4B,C, for $\Delta cheR\Delta cheB$ and for $CheR^+ CheB^+$ cells

1105 respectively. Dashed lines represent $T_{\text{eff}} = 0$ ($CheR^+ CheB^+$) and $T_{\text{eff}} = T$ ($\Delta cheR\Delta cheB$).

1106 Error bars and statistics are as in the main figure.

1107

1108

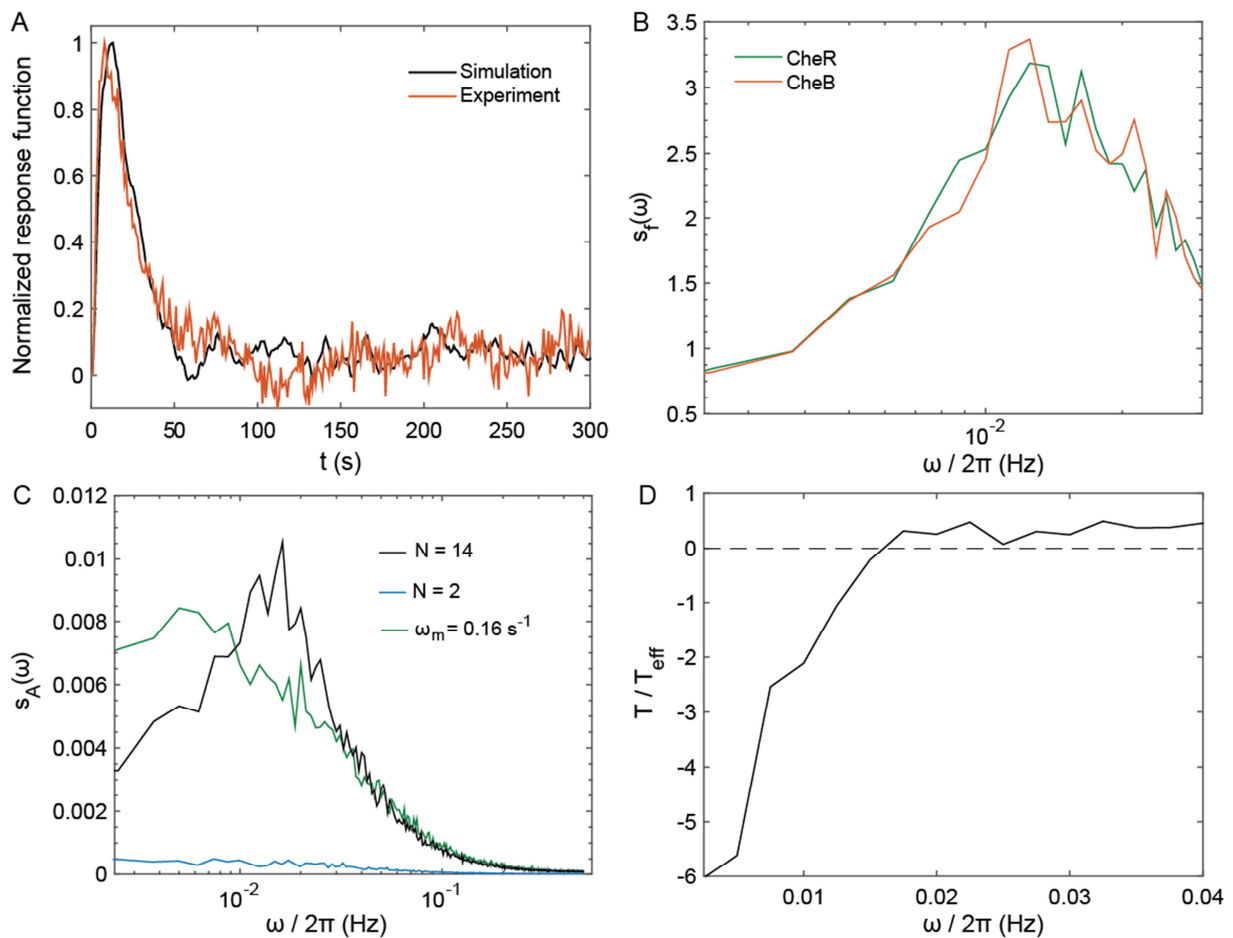


1109

1110 **Figure 4 – Figure Supplement 8. Inferred spectrum of the binding dynamics of CheR and**
1111 **CheB.** Spectrum was calculated in the frequency range where measurement noise is not
1112 dominant, using Equation (A.37). Error bars represent SEM, sample size as in the main figure.

1113

1114



1115

1116 **Figure 4 – Figure Supplement 9. Simulation of the pathway activity fluctuations in**

1117 **adapting cells.** (A) Simulated response function for the model described in section 4 of

1118 Appendix. Comparison with experiments was used to calibrate the time scales of the model. A

1119 unique time scale $\omega_a = 0.25 \text{ s}^{-1}$ was used to model the response of the cluster to free energy

1120 perturbations, averaging fast switching and long-term cluster dynamics, which is then not fully

1121 accounted for in this model (as in Figure Supplement 4). (B) Power spectrum of CheR and CheB

1122 binding to the receptors, showing features similar to its experimental equivalent, plotted in inset

1123 of Figure 4D. (C) The PSD of the level of phosphorylated CheY in the model simulations

1124 (black), which shows similarities with the contribution of methylation-enzymes dynamics to the

1125 PSD of the FRET ratio plotted in main Figure 4D. The PSD amplitude in the simulation was 100
1126 times smaller than its experimental counterpart (since $s_R = \lambda^2 s_A \approx 0.01 s_A$), indicating that
1127 activity perturbations 10 times smaller than in experiment. The PSD was also determined when
1128 the cooperativity was reduced from its standard value of 14 to 2, mimicking the CheW-X2 strain
1129 (blue); and when the specific rate of (de)methylation was decreased from its standard value
1130 $\omega_m = 1$ to 0.16 s^{-1} , mimicking reduced efficiency of (de)methylation in absence of
1131 neighborhood assistance (green). (D) Inverse effective temperature inferred from (A) and (C) in
1132 the simulations, showing behavior similar to the experiments, notably the characteristic sign
1133 inversion as in Figure 4C. Differences emerged at very low frequencies, presumably because the
1134 model does not take long-term receptor array dynamics into account. In the simulated MWC
1135 model of cooperative teams, the fluctuation-dissipation relation can be written for the receptor
1136 team, which leads to effective temperature values similar to the experiments (see Appendix,
1137 section 4).
1138

1139 **Supplementary File S1. List of strains and plasmids used in the study**

1140 Table S1. Strain list

Strain	Genotype	Background	Ref.
VS181	$\Delta(\text{tar}, \text{tsr}, \text{trg}, \text{tap}, \text{aer}) \Delta(\text{cheY}, \text{cheZ})$	RP437	[24]
VH1	$\Delta(\text{tar}, \text{tsr}, \text{trg}, \text{tap}, \text{aer}) \Delta(\text{cheY}, \text{cheZ}) \Delta(\text{cheR}, \text{cheB})$	RP437	[26]
VF7	$\Delta(\text{tar}, \text{tsr}, \text{trg}, \text{tap}, \text{aer}) \Delta(\text{cheY}, \text{cheZ}) \Delta(\text{cheR}, \text{cheB})$ cheW(R117D,F122S)	RP437	[56]
VF8	$\Delta(\text{tar}, \text{tsr}, \text{trg}, \text{tap}, \text{aer}) \Delta(\text{cheY}, \text{cheZ}) \text{cheW(R117D,F122S)}$	RP437	[56]

1141

1142 Table S2. Plasmid list

Plasmid	Genotype	Antibiotic	Induction	Ref.
pVS88	cheY-YFP/cheZ-CFP, pTRC99a derivative	Ampicillin 100 μ g/ml	IPTG 200 μ M,	[24]
pVS1092	Tar ^{QEQE} , pKG110 derivative	Chloramphenicol 17 μ g/ml	Salicylate 2 μ M, If not otherwise stated	[24]
pVS1087	Tar ^{QEEE} , pKG110 derivative	Chloramphenicol 17 μ g/ml	Salicylate 2 μ M, If not otherwise stated	[59]
pVS1086	Tar ^{EEEE} , pKG110 derivative	Chloramphenicol 17 μ g/ml	Salicylate 2 μ M, If not otherwise stated	[57]

1143

1144

1145 **Table 1. Parameters of the FDT analysis**

Parameter	Value
λ	0.10 ± 0.01
N	14
$\langle A \rangle$	0.5
X_A^∞	$N\langle A \rangle(1 - \langle A \rangle)$
N_T	10^4
ϵ_n^2	$0.9 \cdot 10^{-3}$

1146

1147

Appendix

1148

1149 This Appendix presents four partially independent theoretical derivations of equations and
1150 concepts presented in the main text.

1151

1152 **1. Modeling activity fluctuations in the framework of fluctuation-dissipation relation**

1153 *1.1. Fluctuation dissipation relation and effective temperature*

1154 In a system at equilibrium, a fluctuation-dissipation relation links the thermal fluctuations of any
1155 physical quantity to its response to an external small perturbation applied to the system via the
1156 temperature. It extends the corresponding fluctuation-response relation, which links the
1157 amplitudes of the fluctuation and the response, including their evolution in time. For the quantity
1158 a , it reads [64]:

$$-\frac{d}{dt}C_a(t, 0) = kT \frac{\partial \Delta a(t)}{\partial \Delta h(0)}, \quad (\text{A.1})$$

1159 Where:

- 1160 • $C_a(t, 0) = \langle a(t)a(0) \rangle - \langle a(t) \rangle \langle a(0) \rangle$ is the time autocorrelation function of a ,
- 1161 • h is the conjugate of a in the Hamiltonian of the system, that is the Hamiltonian (*i.e.* the
1162 free energy) can be written $H = H_{unperturbed} - ah$
- 1163 • $\frac{\partial \Delta a(t)}{\partial \Delta h(0)}$ is the response of a at time $t > 0$ to the small impulse perturbation Δh applied
1164 transiently at time 0. It is called impulse response function, usually denoted $\chi_a(t)$.

1165 This relation can also be expressed in Fourier space (decomposing all temporal signals in terms
1166 of periodic functions) as: $s_a(\omega) = -\frac{2kT}{\omega} \text{Im} \hat{\chi}_a(\omega)$, where $s_a(\omega)$ is the power spectrum of a and
1167 $\hat{\chi}_a(\omega)$ is the Fourier transform of $\chi_a(t)$, typically referred to as “dynamic susceptibility”.

1168 In a system which is not at equilibrium, but nonetheless at steady state, one can define the so-
 1169 called fluctuation-dissipation ratio [68]:

$$\frac{kT_{\text{eff}}(\omega)}{kT} = -\frac{\omega S_a(\omega)}{2kT \text{Im} \hat{\chi}_a(\omega)}. \quad (\text{A.2})$$

1170 This FDT ratio is a way to quantify some “distance to equilibrium”, introducing the effective
 1171 temperature $T_{\text{eff}}(\omega)$. The system is in equilibrium only if the ratio equals one at all frequencies.

1172

1173 *1.2. Choice of model for the chemotaxis pathway*

1174 We model the receptors by two-state objects, being either kinase activating (ON) or kinase
 1175 inhibiting (OFF). The free energy difference between ON and OFF is $\Delta f_0 = \gamma(m) + \eta(c)$ for a
 1176 single receptor, with $\eta(c) = \ln\left(\left(1 + \frac{c}{K_{\text{OFF}}}\right) / \left(1 + \frac{c}{K_{\text{ON}}}\right)\right)$ being the contribution of attractant
 1177 binding and $\gamma(m) = k_0 - k_1 m$ being the contribution of the receptor methylation.

1178 Two models can describe the coupling between neighboring receptors and kinases in the
 1179 chemoreceptor cluster, the Monod-Wyman-Changeux (MWC) and the Ising models [46, 48, 73,
 1180 91]. The MWC model considers that receptors are grouped by teams of N_{MWC} infinitely coupled
 1181 receptors and their associated kinases. The Hamiltonian of the whole chemoreceptor cluster
 1182 is $H_{\text{MWC}} = \sum_{j=1}^{N_{\text{team}}} (a_j \sum_{k=0}^{N_{\text{MWC}}} \Delta f_0(k))$, a_j being the Boolean state of team j . The Ising model on
 1183 the contrary considers finite coupling between receptors, and the Hamiltonian of the cluster is

$$H_{\text{IM}} = H_{\text{int}} + \sum_{k=1}^{N_T} a_k \Delta f_0(k), \quad (\text{A.3})$$

1184 where a_k is now the state of the single receptor dimer k and H_{int} describes the coupling between
 1185 and among receptors and kinases. The interaction term H_{int} can be written in all generality

1186 $H_{\text{int}} = -J_{aa} \sum_{i,j} (A_i - 0.5) S_{i,j} (A_j - 0.5) - J_{ar} \sum_{i,k} (A_i - 0.5) V_{i,k} (a_k - 0.5) - J_{rr} \sum_{l,k} (a_l -$

1187 $0.5)W_{l,k}(a_k - 0.5)$, where J are the coupling strengths, S , V and W describe the network by
1188 determining whether two components are coupled and A_i is the Boolean activity of the *kinase i*.

1189 **At steady state**, the average activity of the cluster is given in both cases by

$$A = \langle a \rangle = \frac{1}{Z} \iint \frac{1}{N_T} \sum_{k=1}^{N_T} a_k \exp(-\beta H(\{a_k\})) \prod da_k, \quad (\text{A. 4})$$

1190 where Z is a normalization factor, and N_T is the total number of Tar dimers. In the MWC, it is
1191 solved exactly as $A_{MWC} = (1 + \exp(N_{MWC} \Delta f_0))^{-1}$. In the Is, analytical solutions exist only for
1192 a limited set of network topologies, but numerical solutions in most cases are well fitted by

$$A_{Is} = \frac{1}{1 + \exp(N \Delta f_0)}, \quad (\text{A. 5})$$

1193 where N is a fitted parameter, corresponding to an effective ‘‘team size’’, which is proportional
1194 to the average number of neighboring receptors with the same activity (see **I.4**).

1195 The MWC does not allow individual receptors to fluctuate within their team nor any team
1196 rearrangement. This is unsatisfactory since individual receptors are expected to undergo
1197 independent thermal and/or active perturbations and the slow dynamics in the $\Delta cheR \Delta cheB$
1198 strain might come from some remodeling of teams of receptors with the same activity [69]. The
1199 Ising model, which possesses those two properties, was therefore preferred.

1200 Finally, the average methylation state of the receptor evolves under the action of CheR and CheB
1201 according to

$$\frac{dm}{dt} = k_R (1 - A) - k_B A, \quad (\text{A. 6})$$

1202 with k_R and k_B being the rates of methylation and de-methylation, respectively [60].

1203

1204 **1.3. Phenomenological step response function**

1205 To define the effective temperature (Equation (A.2)), the activity state of a *single receptor*
1206 *dimer*, a , will be used as the variable. Considering the definition of the dynamic susceptibility
1207 (paragraph 1.1) and Equation (A.3), within the Ising model, the dynamic susceptibility $\chi_a(t)$ in
1208 response to a perturbation $+\epsilon$ of the free energy difference Δf_0 is

$$\langle \delta a(t) \rangle = \int_{-\infty}^t -\epsilon(\tau) \chi_a(t - \tau) d\tau, \quad (\text{A.7})$$

1209 where $\langle \cdot \rangle$ is an ensemble average. In the case of a constant perturbation ϵ_0 starting at $t = 0$,

$$\langle \delta a(t) \rangle = -\epsilon_0 \int_0^t \chi_a(\tau) d\tau. \quad (\text{A.8})$$

1210 **In the absence of adaptation enzymes**, Equation (A.5) implies that at steady state $\langle \delta a(+\infty) \rangle =$
1211 $-N \langle a \rangle (1 - \langle a \rangle) \epsilon_0$, which yields

$$\int_0^{+\infty} \chi_a^-(\tau) d\tau = N \langle a \rangle (1 - \langle a \rangle) \equiv X_A^\infty. \quad (\text{A.9})$$

1212 Here and in the following, we use a superscript ‘-’ to refer to quantities in the $\Delta cheR \Delta cheB$ case,
1213 and superscript ‘+’ for the $CheR^+ CheB^+$ case.

1214 In the all models so far, the activity switches very rapidly to its steady state value $\langle \delta a(+\infty) \rangle$,
1215 meaning that $\chi_a^-(\tau)$ is well approximated by a delta function. However, as observed in Fig. 4A
1216 of the main text, step stimulation with MeAsp, which corresponds to the application of a constant
1217 ϵ_0 to the receptors, induces also a long term dynamics of the activity, not captured by the
1218 models. A phenomenological description of this long term dynamics was therefore used, leading
1219 to a more complex form of $\chi_a^-(\tau)$.

1220 We experimentally defined the step response function $g^-(t)$, measured as the response of a
 1221 $\Delta cheR\Delta cheB$ strain to small step-like attractant stimulation, as

$$g^-(t) \equiv \frac{\langle \delta a(t) \rangle}{-X_A^\infty \epsilon_0} = \frac{\langle \delta a(t) \rangle}{\langle \delta a(+\infty) \rangle} = \frac{\Delta R(t)}{-\lambda X_A^\infty \epsilon_0} = \frac{\Delta R(t)}{\Delta R(+\infty)}, \quad (A.10)$$

1222 which goes from 0 at $t = 0$ to 1 at $t = +\infty$.

1223 Combining Equations (A.8), (A.9) and (A.10), the dynamic susceptibility of a receptor in
 1224 the $\Delta cheR\Delta cheB$ strain is $\int_0^t \chi_a^-(\tau) d\tau = X_A^\infty g^-(t)$, which is expressed in Fourier space as

$$\hat{\chi}_a^-(\omega) = X_A^\infty i\omega \hat{g}^-(\omega) \quad (A.11)$$

1225 Here the Fourier transform of x is defined as

$$\hat{x}(\omega) = \int_{-\infty}^{+\infty} x(t) e^{-i\omega t} dt \quad (A.12)$$

1226 **In the CheR⁺ CheB⁺ case**, by analogy we experimentally define the step response function to
 1227 small step-like attractant stimulation as:

$$g^+(t) \equiv \frac{\langle \delta a^+(t) \rangle}{-X_A^\infty \epsilon_0} = \frac{\Delta R^+(t)}{-\lambda X_A^\infty \epsilon_0}, \quad (A.13)$$

1228 Here $\Delta R^+(t)$ is the measured YFP/CFP ratio during a small stimulation of free energy ϵ_0 in
 1229 CheR⁺ CheB⁺ cells expressing Tar only and λ is the experimentally determined proportionality
 1230 factor between FRET ratio and activity. Since the response is adaptive, the stimulation
 1231 $-\lambda X_A^\infty \epsilon_0$ cannot be deduced from the final change in FRET ratio ($\Delta R(+\infty)$). It was rather
 1232 computed using $\langle A \rangle = 0.5$ and $\epsilon_0 = \ln(1 + \Delta c/K_{off})$, with $K_{off} = 7 \mu\text{M}$, which is lower than
 1233 the value typically used for WT cells ($K_{off} = 18 \mu\text{M}$) [92], to account for the increased
 1234 sensitivity of the Tar-only strain at our expression level [57].

1235 Similarly to the $\Delta cheRcheB$ case, the following relation holds:

$$\hat{\chi}_a^+(\omega) = X_A^\infty i\omega \hat{g}^+(\omega) \quad (A.14)$$

1236

1237 *1.3.1. Role of CheY/CheZ dynamics*

1238 In the previous sections, we have assumed that the concentration of CheY-P follows
1239 instantaneously the average activity of the cell. In practice, however, [CheY-P] is delayed
1240 compared to the activity. The CheY phosphorylation (by CheA)-dephosphorylation (by CheZ)
1241 cycle can be modeled by [93]:

$$\frac{dy}{dt} = \omega_{AY}A(y_{tot} - y) - \omega_{ZY}Zy \quad (A.15)$$

1242 In Fourier space, assuming that CheZ is abundant, the CheY-P perturbation $\delta y(\omega)$ follows the
1243 activity perturbation as [93]:

$$\delta y(\omega) = \delta y_{max} \frac{\omega_Y}{\omega_Y + i\omega} \delta a(\omega) \quad (A.16)$$

1244 The characteristic frequency is $\omega_Y = 2\text{Hz}$ [93], which lies in the range of frequencies for which
1245 our measurements are dominated by instrumental noise. Therefore CheY/CheZ dynamics was
1246 neglected.

1247 *1.3.2. Effect of diffusive smoothing of the step function*

1248 We assumed a step increase of the attractant concentration when measuring the response
1249 functions. In practice, because of mixing while delivering the media to the cells, the attractant
1250 concentration step is smoothed and it takes about 1 s to reach maximal concentration. We note
1251 $\epsilon(t) = \epsilon_0 \epsilon_s(t)$ the actual experimental free energy change experienced by the cells, with $\epsilon_s(t)$ a
1252 function which is zero for $t < 0$, and rise to 1 in a time scale of the order of 1 s. Typically,
1253 $\epsilon_s(t) = 1 - \exp(-t/\tau_s)$ with $\tau_s = 0.5$ s. In Fourier space, the actually measured activity change
1254 is

$$\langle \delta a_{meas}(\omega) \rangle = -X_A^\infty \epsilon_0 \frac{\chi_a(\omega)}{X_A^\infty} \epsilon_s(\omega) \quad (A.17)$$

1255 Equations (A.7, A.10, A.13) and (A.17) yield a relation between the actually measured response
 1256 functions $g_{meas}^{\pm}(\omega)$ and their ideal counterpart $g_{ideal}^{\pm}(\omega)$ – if the perturbation were purely step-
 1257 like:

$$\frac{\langle \delta a_{meas}(t) \rangle}{-X_A^{\infty} \epsilon_0} \equiv g_{meas}^{\pm}(\omega) = i\omega \epsilon_s(\omega) g_{ideal}^{\pm}(\omega) \quad (A.18)$$

1258 For the typical exponential perturbation, when $\omega \neq 0$,

$$i\omega \epsilon_s(\omega) = 1 - \frac{i\omega \tau_s}{1 + i\omega \tau_s}. \quad (A.19)$$

1259 Equation (A.19) reduces to 1 in the range of frequencies for which our measurement is above
 1260 noise, and $g_{meas}^{\pm}(\omega) = g_{ideal}^{\pm}(\omega)$ was assumed for most of the analysis. Only for measuring the
 1261 time scale of adaptation ω_{RB} and the relation between g^+ and g^- (section 2.1 of this
 1262 supplement) was the full Equation (A.18) needed.

1263

1264 **1.4. Definition of the effective temperature**

1265 Equations (A.2) and (A.11) or (A.14) lead to:

$$\frac{kT_{eff}(\omega)}{kT} = -\frac{s_a(\omega)}{2 X_A^{\infty} Re(\hat{g}(\omega))}, \quad (A.20)$$

1266 Thus, to compute the effective temperature, we need to evaluate the power spectral density
 1267 (PSD) of the activity of a single receptor dimer, $s_a(\omega)$. We experimentally have access to the
 1268 PSD of the YFP/CFP ratio, the fluctuations of which are proportional to the ones of the average
 1269 activity of the cell A_{cell} with the factor λ , modulo the camera noise, so that

$$s_R(\omega) = \lambda^2 s_{A_{cell}}(\omega) + \epsilon_n^2. \quad (A.21)$$

1270 The average activity of the cell is given by $A_{cell} = \frac{1}{N_T} \sum_{k=1}^{N_T} a_k$, so that

$$s_{A_{cell}}(\omega) = \frac{1}{TN_T^2} \sum_{k=1}^{N_T} \sum_{k'=1}^{N_T} \langle \delta a_k(\omega) \delta a_{k'}^*(\omega) \rangle, \quad (\text{A.22})$$

1271 Since receptors are coupled, $\langle \delta a_k(\omega) \delta a_{k'}(\omega) \rangle$ is not necessarily zero. In the Ising model, we
 1272 have $\langle \delta a_k(\omega) \delta a_{k'}^*(\omega) \rangle = \langle |\delta a_k(\omega)|^2 \rangle C(r_{kk'})$, where $C(r_{kk'})$ is the correlation function
 1273 between receptors distant from $r_{kk'}$ on the lattice, which decreases exponentially on a given
 1274 length scale [94], so that $\sum_{k=1}^{N_T} \sum_{k'=1}^{N_T} \langle \delta a_k(\omega) \delta a_{k'}^*(\omega) \rangle = N_T N_r \langle |\delta a_k(\omega)|^2 \rangle$, where N_r is the
 1275 average number of correlated receptors in the cluster (the loose equivalent of the team size of the
 1276 MWC model), which is expected to be proportional to the cooperativity number N (Equation
 1277 A.5).

1278 To accurately count the number of correlated receptors, we noted that recent works measured *in*
 1279 *vitro* [63] and *in vivo* [44, 56] the response function of the minimal functional chemosensory
 1280 assembly, believed to consist of two trimers of receptor dimers (TD) coupled to one CheA dimer,
 1281 and found a cooperativity number close to 2. The dose-response curve of $\Delta cheR \Delta cheB$ CheW-
 1282 X2 expressing Tar^{QEQE}, featuring such minimal complexes [44, 56], was fitted using Equation
 1283 (A.5) (Figure 3 – Figure Supplement 1), also yielding $N \approx 2$. These results strongly suggest that N
 1284 effectively accounts for the number of TDs coupled in a “signaling team”, thus $N_r = 3N$ and:

$$s_{A_{cell}}(\omega) = \frac{3N}{N_T} s_a(\omega) \quad (\text{A.23})$$

1285 Finally, Equations (A.9), (A.20), (A.21) and (A.23) yield:

$$\frac{kT_{\text{eff}}(\omega)}{kT} = -\frac{N_T}{6\lambda^2 N^2 A(1-A)} \frac{s_R(\omega) - \epsilon_n^2}{\text{Re}(\hat{g}(\omega))}, \quad (\text{A.24})$$

1286 corresponding to Equation (1) and (2) of the main text, which defines the dissipation $G_R(\omega) =$
1287 $-2 \lambda^2 \frac{3N^2 A(1-A)}{N_T} \text{Re}(\hat{g}(\omega))$.

1288 Note that although we expressed the fluctuation dissipation relation in terms of activity, which
1289 allows us to directly compare the analysis with experimental data, this relation can be formulated
1290 for any variable (e.g., receptor conformation) that itself determines the activity.

1291 **2. Link between the response functions in $\Delta cheR\Delta cheB$ and $CheR^+ CheB^+$ cases**

1292 In presence of the adaptation system, the receptor cluster is assumed to respond to free energy
 1293 perturbations in the same way as in the adaptation-deficient cells, but this response induces a
 1294 methylation change adding up to the free energy perturbation. In Fourier space, for a small
 1295 perturbation of the free energy difference $\epsilon(\omega)$, the resulting perturbations for the average
 1296 activity and methylation are then given – from Equations (A.6) and (A.7) – by the set of
 1297 equations:

$$\langle \delta a^+(\omega) \rangle = X_A^\infty i\omega \hat{g}^-(\omega) (-\epsilon(\omega) + k_1 \langle \delta m(\omega) \rangle) \quad (A.25)$$

$$i\omega \langle \delta m \rangle = -(k_R + k_B) \langle \delta a^+(\omega) \rangle \quad (A.26)$$

1298 Defining $\omega_{RB} = X_A^\infty k_1 (k_R + k_B)$, the activity dependent rate of adaptation, this set of equations
 1299 is easily solved as

$$\langle \delta a^+(\omega) \rangle = \frac{X_A^\infty i\omega \hat{g}^-(\omega)}{1 + \omega_{RB} \hat{g}^-(\omega)} (-\epsilon(\omega)) \quad (A.27)$$

1300 We thus inferred the dynamic susceptibility in $CheR^+ CheB^+$ as

$$\hat{\chi}_a^+(\omega) = \frac{X_A^\infty i\omega \hat{g}^-(\omega)}{1 + \omega_{RB} \hat{g}^-(\omega)} \quad (A.28)$$

1301 Note that the $\Delta cheR\Delta cheB$ case is obtained again if $\omega_{RB} = 0$.

1302 From Equation (A.14), the step response functions in the $CheR^+ CheB^+$ and $\Delta cheR\Delta cheB$ cases
 1303 are linked by:

$$\hat{g}^+(\omega) = \frac{\hat{g}^-(\omega)}{1 + \omega_{RB} \hat{g}^-(\omega)} \quad (A.29)$$

1304

1305 **2.1. Effect of diffusive smoothing of the step function**

1306 In the case where the stimulation is not a perfect step function, modeled by $\epsilon(\omega) = \epsilon_0 \epsilon_s(\omega)$,
1307 using Equations (A.17) and (A.18), the relation of equivalence can be easily shown to become:

$$\hat{g}_{meas}^+(\omega) = \frac{i\omega \epsilon_s(\omega) \hat{g}_{meas}^-(\omega)}{i\omega \epsilon_s(\omega) + \omega_{RB} \hat{g}_{meas}^-(\omega)}. \quad (\text{A.30})$$

1308 Using $\epsilon_s(t) = 1 - \exp\left(-\frac{t}{\tau_s}\right)$, with $\tau_s = 0.5$ s, the equivalent of Equation (A.30) in real space
1309 was fitted using the experimentally determined $\hat{g}_{meas}^-(\omega)$ and $\hat{g}_{meas}^+(\omega)$, with ω_{RB} as a free
1310 parameter, yielding $\omega_{RB} = 0.06$ Hz (Figure 4 - Figure Supplement 5).

1311

1312 **2.2. Frequency of effective temperature divergence**

1313 In the CheR⁺ CheB⁺ case, the effective temperature diverges when $\text{Re}\hat{g}^+(\omega) = 0$. Equation
1314 (A.29) thus yield an implicit equation for the frequency at which this divergence occurs,
1315 $-\text{Re}g^-(\omega_{divg}) = \omega_{RB} |g^-(\omega_{divg})|^2$, which has a solution since $\text{Re}g^-(\omega)$ is negative. This
1316 equation clearly represents a balance between the action of the cluster cooperative response
1317 (represented by g^-) and adaptation (represented by ω_{RB}). The solution is however not trivial, in
1318 particular $\omega_{divg} \neq \omega_{RB}$, and will depend on both the time scales of cluster dynamics and
1319 adaptation. Notably, in [74] the typical time scale of the cluster dynamics was chosen to be much
1320 shorter than the one suggested by our measurements, resulting in higher frequency of effective
1321 temperature divergence.

1322

1323 **3. Separating the contribution of methylation enzymes dynamics to the PSD in CheR⁺**
 1324 **CheB⁺ cells**

1325 A complementary approach to the modeling of the fluctuating activity of chemoreceptor clusters,
 1326 which has been used in a number of previous theoretical works [75-77], is to introduce noise
 1327 terms in equations (A.25) and (A.26), which describe the average behavior of the system, in
 1328 order to describe the behavior of single receptor k :

$$\delta a_k(\omega) = X_A^\infty i\omega \hat{g}^-(\omega) (-\epsilon_k(\omega) + k_1 \delta m_k(\omega)) \quad (A.31)$$

$$i\omega \delta m_k = - (k_R + k_B) \delta a_k(\omega) + \delta r_k(\omega) + \delta b_k(\omega) \quad (A.32)$$

1329 Here $\epsilon_k(\omega)$ represents thermal noise acting on the receptor, and $\delta r_k(\omega)$ and $\delta b_k(\omega)$ represent
 1330 noise coming from the intermittent action of CheR and CheB, respectively (see below for
 1331 possible interpretation of these fluctuations).

1332 This set of equations is easily solved as

$$\delta a_k(\omega) = X_A^\infty \hat{g}^+(\omega) (-i\omega \epsilon_k(\omega) + k_1 (\delta r_k + \delta b_k)), \quad (A.33)$$

1333 where $\hat{g}^+(\omega)$ is defined by Equation (A.29), and can be measured using Equation (A.13).

1334 Assuming that the power spectra of δr_k and δb_k are identical, denoted $s_{rb}(\omega)$, the power
 1335 spectrum of the activity of one receptor is:

$$s_a^+(\omega) = |X_A^\infty \hat{g}^+(\omega)|^2 (\omega^2 s_\epsilon(\omega) + 2k_1^2 s_{rb}(\omega)). \quad (A.34)$$

1336 This equation highlights the contributions of thermal fluctuations and methylation noise to the
 1337 PSD. If the methylation system is absent, this latter equation reduces to the $\Delta cheR \Delta cheB$ case:

$$s_a^-(\omega) = |X_A^\infty \hat{g}^-(\omega)|^2 \omega^2 s_\epsilon(\omega). \quad (\text{A.35})$$

1338 Under the non-trivial assumption that the thermal noise term (which can be explicitly evaluated
 1339 using the FDT, Equation (A.20)) remains the same whether adaptation enzymes are present or
 1340 not, the contribution of the enzymes to the PSD in CheR⁺ CheB⁺ is:

$$s_a^m(\omega) = s_a^+(\omega) - \left| \frac{g^+(\omega)}{g^-(\omega)} \right|^2 s_a^-(\omega) = |k_1 X_A^\infty \hat{g}^+(\omega)|^2 s_{rb}(\omega), \quad (\text{A.36})$$

1341 which yields in terms of the FRET ratio, from equations (A.21) and (A.23):

$$s_R^m(\omega) = s_R^+(\omega) - \left| \frac{g^+(\omega)}{g^-(\omega)} \right|^2 s_R^-(\omega) = \frac{3N\lambda^2}{N_T} |k_1 X_A^\infty \hat{g}^+(\omega)|^2 s_{rb}(\omega). \quad (\text{A.37})$$

1342 Here the thermal noise contribution in presence of adaptation is $s_R^T(\omega) = \left| \frac{g^+(\omega)}{g^-(\omega)} \right|^2 s_R^-(\omega)$.

1343 **3.1. Possible interpretation of the methylation-based noise term**

1344 The non-perturbative equation for the evolution of the methylation of receptor k reads:

$$\frac{dm_k}{dt} = -w_b b_k a_k + w_r b_r (1 - a_k) \quad (\text{A.38})$$

1345 Here b_k and r_k evaluate whether, respectively, CheB or CheR is present on the site to act on the
 1346 receptor, with respective rates w_b and w_r , in an activity-dependent manner. This equation
 1347 accounts for the fact that CheR and CheB, which are in low amounts compared to the total
 1348 amount of receptors, bind and unbind in the vicinity of only a given number of receptors. Hence
 1349 not all receptors are (de)methylated at a given time [33]. The ensemble average of equation
 1350 (A.38), describing the average methylation dynamics, is:

$$\frac{d\langle m \rangle}{dt} = -w_b \frac{N_B}{N_T} \langle A \rangle + w_r \frac{N_R}{N_T} (1 - \langle A \rangle) \quad (\text{A.39})$$

1351 This identifies the ensemble averaged rate of (de)methylation, $k_R = w_r \frac{N_R}{N_T}$ ($k_B = w_b \frac{N_B}{N_T}$).

1352 Subtracting equation (A.39) from equation (A.38) leads to the perturbative equation (A.32). This

1353 enables to define δb_k and δr_k as:

$$\delta r_k = w_r (1 - \langle A \rangle) \left(r_k - \frac{N_R}{N_T} \right) \quad (\text{A.40})$$

$$\delta b_k = w_b \langle A \rangle \left(b_k - \frac{N_B}{N_T} \right) \quad (\text{A.41})$$

1354 These equations enable to identify δr_k (δb_k) as the fluctuations in occupancy of a given receptor

1355 by CheR (CheB) and thus $s_{rb}(\omega)$ as the power spectrum of enzyme binding dynamics.

1356 Although noisy, $s_{rb}(\omega)$ appeared to decrease at low frequency (Figure 4 – Figure Supplement

1357 8). Such a decrease indicates anti-correlations [95] in the binding dynamics of the methylation

1358 enzymes at their substrates, which is consistent with the common assumption that CheR (CheB)

1359 loads and acts only on the inactive (active) receptor. For the example of CheR, this activity

1360 dependence implies that once receptor is active, it will not allow CheR to reload and restart

1361 acting until it switches back into the inactive state, thus introducing a delay in the rebinding of

1362 the enzyme. As a consequence, enzyme binding anti-correlates on the time scale of this delay.

1363

1364 4. Simulation of a simplified model for the array of receptors

1365 In order to reproduce semi-qualitatively the features of the $\text{CheR}^+ \text{CheB}^+$ behavior displayed in
1366 Figure 4, a simple model of the receptor array was simulated. The standard values of all
1367 simulation parameters are given in Appendix – Table 1. The simulated array is composed of
1368 $N_{\text{team}} = 300$ independent MWC signaling teams. The MWC model was chosen for simplicity,
1369 and it is expected to lead to qualitative but not necessarily quantitative match between
1370 simulations and experiments. Each signaling team is composed of $N_{rcp} = 3N$ receptor dimers –
1371 each of which counts 8 methylation sites. The Boolean activity a_k of the signaling team evolves
1372 according to:

$$\frac{da_k}{dt} = -w_a \left(a_k - \frac{1}{1 + e^F} \right), \quad F = N \Delta f_0 - k_1 (m_k - N_{rcp} m_0) \quad (\text{A.42})$$

1373 Here, Δf_0 is the attractant dependant stimulation, w_a is the flipping rate of the kinase and m_k is
1374 the total methylation level of the team.

1375 If m_k is fixed, Equation (A.42) is a simple model for the $\Delta cheR \Delta cheB$ case. Since the activity of
1376 a single team can only take 0 or 1 as a value, it fluctuates between these two values, being only
1377 on average equal to $1/(1 + e^F)$. Since the teams are uncoordinated, the average activity of the
1378 whole cluster will fluctuate as well. This dynamics represents the thermal fluctuations in a MWC
1379 model. This dynamics was simulated for $T = 1000$ s after an equilibration period from a random
1380 initial condition of same duration, for $n = 100$ repeats, with $F = 0$, *i.e.* $\langle a \rangle = 0.5$. Increasing
1381 latencies in the response to stimulations of the receptor cluster were modeled by decreasing w_a ,
1382 for a fixed amplification factor $N = 14$. As expected, the thermal fluctuations were slower for
1383 lower w_a . The maximal amplitude of the fluctuations was also larger when w_a was larger (Figure

1384 4 – Figure Supplement 4). Increasing N while keeping the total number of receptors constant (*i.e.*
 1385 decreasing N_{team} accordingly), at fixed w_a , led to an increased amplitude of the fluctuations,
 1386 their temporal dependences being however not affected (Figure 4 – Figure Supplement 4). The
 1387 power spectra however differed from experimental data. The amplitude was underestimated
 1388 because the MWC does not allow applying thermal fluctuations to individual receptor. The time
 1389 dependence was also different because we modeled the slow receptor cluster dynamics by
 1390 lengthening the switching rate w_a , which is the only time scale of the model, where in reality
 1391 they probably are different processes.

1392 In the $CheR^+ CheB^+$ case, the methylation level evolves according to:

$$\frac{dm_k}{dt} = w_m \left(r_k \&(m_k < 8N_{rcp}) - b_k \&(m_k > 0) \right) \quad (A.43)$$

1393 Here r_k (b_k) represents whether a CheR (CheB) protein is tethered to the team. Importantly, the
 1394 model assumes that only one enzyme may be tethered to the team at a time. (De)methylation
 1395 occurs at the rate w_m if CheR (CheB) is present and m_k has not reached its maximal (minimal)
 1396 value. The enzyme tethering dynamics is given by the set of equation:

$$\frac{dr_k}{dt} = w_l(1 - r_k)(1 - b_k)(1 - a_k) - w_u r_k a_k \quad (A.44)$$

$$\frac{db_k}{dt} = w_l(1 - r_k)(1 - b_k)a_k - w_u b_k(1 - a_k) \quad (A.45)$$

1397 under the constraint $\sum_k b_k \leq b_{tot}$ and $\sum_k r_k \leq r_{tot}$. This means that CheR (CheB) may only
 1398 load, if free enzymes are available, on free inactive (active) receptors with rate w_l and unload
 1399 once the receptor turned active (inactive) with rate w_u .

1400 The typical dynamics in the simulation will then be the following. Take, for example, a weakly
1401 methylated team. Its activity will get to zero (Equation (A.42)). If free CheR is available, it will
1402 load on the team (Equation (A.44)) and methylate it (Equation (A.43)), until the methylation
1403 level is high enough to activate the team (Equation (A.42)). CheR will then unload (Equation
1404 (A.44)), and a hypothetical free CheB can then load on the team (Equation (A.45)) to demethylate
1405 it and bring it to its initial state.

1406 The level of phosphorylated CheY of the simulated cell, also used as an output of the model,
1407 evolves according to:

$$\frac{dy}{dt} = w_y \left(\frac{1}{N_{team}} \sum_{k=1}^{N_{team}} a_k - y \right) \quad (A.46)$$

1408 Output quantities were averaged over $n = 100$ independent simulations of single cells.

1409 In practice, w_u , w_l and w_a were chosen of the same order of magnitude, and they were the
1410 slowest dynamics, whereas w_m was the fastest, in order to obtain reasonable dynamics.

1411 Starting from a random initial condition, the system was let to equilibrate at $\Delta f_0 = 0$ for 100
1412 times the slowest time scale of the system ($1/w_l$). The system was then challenged with free
1413 energy perturbation $\Delta f_0 = \ln(1 + 0.3/7)$ (mimicking the experimental conditions) to measure
1414 the step response function, computed as $g_{simu}(t) = \frac{\Delta y(t)}{N_{eff} \Delta f_0}$. Figure 4 – Figure Supplement 9A
1415 shows the normalized step response function compared to its experimental counterpart with
1416 excellent agreement (although absolute amplitudes differed moderately).

1417 A $T = 800$ s equilibrated run was further used to compute power spectra, using Equation (5) of
1418 the main text. The power spectra of r_k and b_k , corresponding to the inferred $s_{rb}(\omega)$ defined in

1419 Equation (A.36), show good qualitative agreement with the experimental data, with a transition
1420 from high values at frequencies larger than 0.01 Hz to low values below this threshold (Figure 4
1421 – Figure Supplement 9B). This transition indicates anti-correlations in the occupancy of the
1422 receptor teams by the enzymes, which emerge from their *activity-dependant* loading and
1423 unloading. The two spectra are equal within noise by construction of the model (r and b play
1424 symmetric roles). Furthermore, the simulated power spectrum of the activity $s_A(\omega)$ was similar
1425 to the experimental power spectrum corrected for long term cluster dynamics (compare Figure
1426 4D with Figure 4 – Figure Supplement 9C). The amplitude of the power spectrum was however
1427 ~100 fold lower than in experiments, but in line with previous simulations [74].

1428 Finally, from the power spectrum of the CheY-P level $s_Y(\omega)$, which was very close to $s_A(\omega)$, an
1429 effective temperature can be computed as

$$\frac{T}{T_{\text{eff}}} = \frac{2\langle A \rangle(1 - \langle A \rangle)}{N_{\text{team}}} \frac{\hat{g}_{\text{simu}}(\omega)}{s_Y(\omega)} \quad (\text{A.47})$$

1430 It compares qualitatively well with the experimental effective temperature, with concordant
1431 frequencies of divergence (Figure 4 – Figure Supplement 9D). Differences appear for the lowest
1432 frequencies, probably because of the long-term dynamics of the receptor clusters, which was not
1433 accounted for by these simulations.

1434 All things being otherwise equal, modifying N to 2 and N_{team} to 2100, which models the
1435 disruption of the chemoreceptor clusters into individual trimers of dimers, reduced strongly the
1436 fluctuations in activity (Figure 4 – Figure Supplement 9C). Decreasing the specific rate of
1437 receptor (de)methylation when the enzyme is bound to the receptors, w_m , to $w_m = 0.016 \text{ s}^{-1}$ had
1438 however little effect (Figure 4 – Figure Supplement 9C). Note that in both cases the adaptation

1439 time is reduced by a similar factor (7 and 6, respectively), since this time is proportional to the
1440 product $N\omega_m$, as evident from equations (A.41) and (A.42).

1441 Conditional tethering of the adaptation enzymes to the receptors therefore seems to account
1442 relatively well for the observed dynamics. One important discrepancy between simulations and
1443 experiments is in the amplitudes of the fluctuations, which are much larger than expected in
1444 experiments, when the simple MWC model is considered.

1445 **Appendix-Table 1**

Parameter	Value	Reference
N	14	This study (based on experimental values)
N_{team}	300	This study (based on experimental values)
k_1	0.016	Adapted from [96]
w_m	1 s^{-1}	This study
w_l	0.15 s^{-1}	This study
w_u	0.5 s^{-1}	This study
w_y	1 s^{-1}	[93]
w_a	0.25 s^{-1}	This study
b_{tot}	240	[29]
r_{tot}	140	[29]

1446